# NASA TECHNICAL MEMORANDUM 104089
# USAAVSCOM TECHNICAL REPORT 91-B-009

# DAMAGE PREDICTION IN CROSS-PLIED CURVED COMPOSITE LAMINATES

**Roderick H. Martin**
**and**
**Wade C. Jackson**



**JULY 1991**

National Aeronautics and Space Administration

**Langley Research Center**
Hampton, Virginia 23665

US ARMY
AVIATION
SYSTEMS COMMAND
AVIATION R&T ACTIVITY

## SUMMARY

This paper details the analytical and experimental work required to predict delamination onset and growth in a curved cross-plied composite laminate subjected to static and fatigue loads. The composite used was AS4/3501-6, graphite/epoxy. Analytically, a closed form stress analysis and 2-D and 3-D finite element analyses were conducted to determine the stress distribution in an undamaged curved laminate. The finite element analysis was also used to determine values of strain energy release rate at a delamination emanating from a matrix crack in a 90° ply. Experimentally, transverse tensile strength and fatigue life were determined from flat 90° coupons. The interlaminar tensile strength and fatigue life were determined from unidirectional curved laminates. Also, mode I fatigue and fracture toughness data were determined from double cantilever beam specimens. Cross-plied curved laminates were tested statically and in fatigue to give a comparison to the analytical predictions. A comparison of the fracture mechanics life prediction technique and the strength based prediction technique is given.


## NOMENCLATURE

| | |
|---|---|
| $a_o$ | initial delamination length |
| $a$ | delamination length |
| A,B,C,D | constants in curve fit expression |
| $E_{11}$ | elastic modulus in the fiber direction |
| $E_{22}$ | elastic modulus transverse to fiber direction |
| $E_{33}$ | elastic modulus through thickness |
| $f$ | frequency |
| $G$ | total strain energy release rate |
| $G_c$ | critical value of strain energy release rate |
| $G_{Ic}$ | mode I static interlaminar fracture toughness |

| | |
|---|---|
| $G_{Imax}$ | maximum mode I cyclic strain energy release rate |
| L | moment arm length |
| m | constant in DCB compliance expression |
| n | exponent in DCB compliance expression |
| P | load |
| $P_{max}$ | maximum cyclic load |
| $P_{min}$ | minimum cyclic load |
| R | radius |
| $R_{inner}$ | inner radius |
| t | thickness |
| w | width |
| z | width wise coordinate |
| $\alpha$ | delamination angle counter clockwise |
| $\beta$ | delamination angle clockwise |
| $\delta_{max}$ | maximum cyclic displacement |
| $\delta_{min}$ | minimum cyclic displacement |
| $\theta$ | angle around curved portion of laminate |
| $\sigma_r$ | radial stress |
| $\sigma_\theta$ | tangential stress |
| $\sigma_{2c}$ | transverse static strength |
| $\sigma_{2max}$ | transverse cyclic stress |
| $\sigma_{3c}$ | interlaminar static strength |
| $\sigma_{3max}$ | interlaminar cyclic stress |
| $\tau_{r\theta}$ | interlaminar shear stress |
| $\upsilon_{12}$ | Poisson's ratio |

## INTRODUCTION

Many laminated composite structures, such as an angle bracket or a co-cured web or a frame have a loaded curved portion [1], fig. 1. The final failure in such structures may be a complex progression of ply cracking, delamination and fiber failure. Delamination may initiate from radial stresses caused by the bending. Also, any tangential stresses present may cause matrix cracks to develop in an off-axis ply. If a crack occurs, singular interlaminar stresses will be created where the matrix crack meets the adjacent plies. These interlaminar stresses may create local delaminations, shown schematically in fig. 1. The difference in

material properties between adjacent plies of different orientation may also cause mathematically singular stresses at the free edges which may initiate edge delaminations. These edge delaminations may interact with the previously mentioned failure modes and complicate delamination onset predictions using classical strength based failure criteria. Therefore, the need to understand the stress distribution and damage mechanisms in a curved laminate is important in aiding the structural designer to predict the strength of such a component.

To extend strength prediction techniques to account for singular stresses from matrix cracks, delaminations, material defects, edges or any other discontinuity, a fracture mechanics prediction capability is necessary. Interlaminar fracture mechanics based failure criteria offer a technique to predict the onset and growth of delamination in a component with a singular stress source [2-8]. For an interlaminar fracture mechanics based failure criterion, a value of strain energy release rate, G, must be determined at every potential delamination source. This value of G may be termed the critical value, $G_c$, and will cause delamination onset and growth when it equals the interlaminar fracture toughness of the composite. The techniques to determine the critical value of G may depend on the source of the potential delamination.

Figure 2 gives some examples of how $G_c$ was determined for different structures. For edge delamination in a flat

multidirectional laminate, G increased from zero to a plateau within a few ply thicknesses from the edge, fig. 2a [2]. The value of G at the plateau was used to predict delamination onset at the edge. In a tapered laminate, the peak value of G was used to predict delamination onset, fig. 2b [3]. For delamination growth from a matrix crack in a curved laminate [6], the point of inflection in the G versus delamination length curve was postulated to give the critical value of G required to predict static delamination onset, fig. 2c. The effect of the free edge on the growth of local delaminations initiating from a matrix crack in a flat laminate subjected to tensile loads was investigated in ref. 7. For a straight delamination front perpendicular to the edge, the value of G increased to a plateau value as the delamination grew from the matrix crack. This plateau was assumed to give the critical value of G similar to the edge delamination case, fig. 2a. A curved laminate was analyzed with a delamination emanating from a matrix crack in ref. 8. The G versus delamination length curve was extrapolated to zero delamination length to determine a critical value of G, fig. 2d.

The purpose of this paper is to predict damage in a curved laminate subjected to static and fatigue loads using a strength and a fracture mechanics based failure criterion. The stress distribution in an undamaged cross-plied curved laminate was determined using a closed form solution and a 2-D and 3-D finite element analyses (FEA). The G distribution for a delamination

initiating from a matrix crack in a set of 90° plies was determined from the 2-D and 3-D finite element analyses. Static and fatigue tests were conducted using flat 90° laminates to determine the transverse strength, $\sigma_{2c}$, and the fatigue life. Unidirectional curved laminates were used to determine interlaminar tensile strength, $\sigma_{3c}$ and the fatigue life. The mode I interlaminar fatigue and fracture toughnesses of the composite material were determined using a unidirectional double cantilever beam (DCB) specimen. Attempts to predict interlaminar tension delamination of the cross-plied curved laminate were made by comparing the maximum radial stress to the interlaminar tensile strength and life data for the composite. Attempts to predict matrix cracking were made by comparing the maximum radial and tangential stress in a 90° ply to the transverse and interlaminar strength and life data. Finally, attempts to predict delamination onset from a matrix crack were made by comparing the appropriate values of G to the fatigue and fracture toughness data. Static and fatigue tests were also conducted on a cross-plied curved laminate to determine the damage modes and static and fatigue strength to compare with the predictions.

In addition to the curved laminate being used as a structural component, it has been considered as a possible test specimen to determine the interlaminar tensile strength, $\sigma_{3c}$, for composite materials [9]. Therefore, it is a secondary objective of this paper to determine whether or not the multidirectional curved

laminate is suitable for $\sigma_{3c}$ determination considering the additional damage modes that may be present and the difficulty in determining stresses at singularities.

## EXPERIMENTAL PROCEDURE AND RESULTS

This section describes the materials, the experimental procedure and experimental results. All specimens were fabricated from Hercules AS4/3501-6 graphite/epoxy. The specimens were cured in an autoclave according to the manufacturer's recommendations. Material elastic moduli were obtained from ref. 4 and were

$E_{11}$ = 140 GPa $\qquad$ $E_{22} = E_{33}$ =11.0 GPa

$G_{12} = G_{13}$ = 5.84 GPa $\qquad$ $\upsilon_{12}= \upsilon_{13}$=0.3

The volume fractions for each specimen type are given in their corresponding subsections below. Prior to testing, all specimens were dried using the following cycle: 1 hour at 95°C, 1 hour at 110°C, 16 hours at 125°C and 1 hour at 150°C. Following the drying cycle, the specimens were stored in a desiccator cabinet until tested.

### Transverse Tension Strength Tests

Flat 90°, unidirectional, 24-ply specimens were fabricated for the transverse tension tests. The specimen dimensions were 150 X 33mm with the fibers oriented in the 33mm width direction. The specimens had a volume fraction of 65.0 percent. The specimens were subjected to static tests and to load controlled fatigue tests at an R-ratio ($P_{min}/P_{max}$) of R=0.1 and at a frequency of 5Hz. The tests were conducted until failure occurred. In most of these

tests no loading tabs were used, and most specimens failed at or near the grips. In a few specimens glass epoxy loading tabs were used. However the failures were still at or near the grips, so the use of tabs was discontinued. The static failure load or the number of cycles to failure was recorded and the results are shown in fig. 3. The straight lines were drawn through the data to represent the lower and upper bound curves between $10^2$ and $10^6$ cycles. The use of these fits will be described later. The arrows on the fatigue data points in fig. 3 and subsequent figures indicate that the specimen did not fail.

**Interlaminar Tension Strength Tests**

Unidirectional, 0° curved laminate specimens were fabricated for interlaminar tensile strength determination. The specimens had 24 plies and their configuration and dimensions are given in fig. 4. The pre-preg was laid over a solid aluminum block and the panels cured in an autoclave. The specimens had an average volume fraction in the curved region of 54.7 percent. The static strengths of these specimens were taken from ref. 4. Fatigue tests were conducted using the test fixture shown in fig. 5. The fatigue tests were conducted under load control at an R-ratio of 0.1 and a frequency of 5Hz. The number of cycles to the onset of delamination was noted. The onset of delamination also corresponded to a rapid loss of bending stiffness of the curved portion. At the loss of bending stiffness the machine hydraulics and the cyclic counter switched off. From ref. 4 the maximum

normalized radial stress was determined to be ($\sigma_r$ w/P) = 4.37 $mm^{-1}$, occurring near the mid-thickness of the curved region. The tangential and in-plane shear stresses were negligible at this location. This value of radial stress was used with the applied loads to determine $\sigma_{3max}$ (or $\sigma_{3c}$) using eq. 1.

$$\sigma_{3max} = \left(\frac{\sigma_r\, w}{P}\right)\left(\frac{P_{max}}{w}\right) = 4.37\left(\frac{P_{max}}{w}\right) \qquad (1)$$

The fatigue results from this work and the static results from ref. 4 are shown in fig. 6. The straight lines were drawn through the data to represent the lower and upper bound curves between $10^2$ and $10^6$ cycles. The use of these fits will be described later.

**Double Cantilever Beam Tests**

Double cantilever beam (DCB) specimens were fabricated to determine the mode I fatigue and static fracture toughness of the composite. The specimens were 24-ply, 0° unidirectional laminates. A 13$\mu$m non-adhesive Kapton film was placed at the mid-plane at one end prior to curing to simulate a delamination. The specimen dimensions were 100 X 25mm. The specimens had a volume fraction of 55.9 percent. Piano hinges were bonded to the surface to allow load to be transferred to the beam. The static tests were conducted under displacement control at a loading rate of 0.5mm/min. Fracture toughness, $G_{Ic}$, was determined for a delamination initiating from the end of the thin insert [10]. The fatigue tests were conducted under displacement control at an

R-ratio ($\delta_{min}/\delta_{max}$) of R=0.1, at a frequency of 5Hz at various maximum cyclic displacements [10,11]. The number of cycles to delamination onset was determined by monitoring the maximum cyclic load, $P_{max}$. If a 1 percent decrease in $P_{max}$ was observed then the delamination was assumed to have grown. Delamination onset was also monitored by visual inspection of the tip of the insert. Figure 7 shows the fracture toughness and the maximum cyclic strain energy release rate, $G_{Imax}$, versus the number of cycles to delamination onset, where $G_{Imax}$ was calculated from

$$G_{Imax} = \frac{n\, P_{max}\, \delta_{max}}{2\, w\, a_0} \qquad (2)$$

where n is the exponent in the static compliance expression $\delta/P = ma^n$ (an average value of n= 2.58 from three specimens was used in equation 2), and $a_0$ is the initial delamination length. The visual and 1 percent load drop methods of determining the number of cycles to delamination onset gave inconsistent results. The visual detection method gave lives greater, less than and similar to the 1 percent load drop method. In some specimens a 1 percent load drop was not detected after visual delamination growth had been observed. Hence, the visual data was used in the predictions presented later.

**Cross-Plied Curved Laminate Tests**

Static and fatigue tests were conducted on cross-plied curved laminates. The cross-plied specimens were laid up to the

dimensions given in fig. 4 using the same procedure described for the unidirectional curved laminates above. The lay-up used was $[0_4/90_3/0_5]_s$ and will be referred to as lay-up A. This particular lay-up was chosen because it was anticipated that a matrix crack would occur in the tension loaded 90° plies and that delamination would grow from the matrix crack. The lay-up was not intended to represent a viable lay-up for a structural component. The specimens had a volume fraction of 59.5 percent in the curved region. During the static and fatigue tests the first audible sign of damage corresponded to complete loss of bending stiffness of the curved portion of the specimen.

The results of the static and fatigue tests on lay-up A are shown in fig. 8. The fatigue results are plotted as the maximum applied load per unit width versus number of cycles to onset of damage. The static results of ref. 6 are also shown in fig. 8. The lay-up used in that work was $[0_4/90_3/0/90_2/0_2]_s$ and is referred to as lay-up B. The failure paths for lay-ups A and B are shown in figs. 9 and 10 respectively. In fig. 9, an oblique matrix crack can be seen in the tension loaded $[90]_3$ plies with delaminations emanating from this crack. Other delaminations consistent with an interlaminar tension failure can be seen in the 0° plies. In fig. 10 a straight matrix crack can be seen in the tension loaded $[90]_3$ plies and also in the $[90]_2$ plies above. This second matrix crack, which was not analyzed in ref. 6, was another reason lay-up A was chosen for this work, i.e. to eliminate the complications of

two matrix cracks in the analysis.

## ANALYSIS

This section details the analysis conducted on the cross-plied curved laminates to determine the stress distribution with no damage present and the strain energy release rate distribution with matrix ply cracking and delamination present. The stress analysis consists of a closed form multilayer theory. These results are compared with a 2-D and a 3-D finite element analysis. The finite element analysis was also used to determine the G distribution. In the finite element models and the closed form solution, residual thermal and moisture stresses were not considered.

### 2-D Closed Form Solution

Classical anisotropic elasticity theory was used to construct a multilayered theory to calculate stresses and deformation fields around the curved laminate using the method in ref. 12. Both an end moment and an end force were applied to a quarter section of a circular beam. An Airy stress function was written in cylindrical coordinates for each layer in the beam. At every interface between layers, both the displacements and stresses were matched to the adjacent layer to assure continuity and equilibrium between layers. The boundary conditions for the inner and outer surfaces were traction free. At the end of the beam, the end force and end moment were balanced by the shear and tangential stresses, respectively. The total stress in the beam is a summation of the stresses caused by the end force and the moment. Once the

constants in the Airy stress function were known, the stresses were determined at any location $(R,\theta)$ in the beam using the expressions in ref. 12.

**Finite Element Analysis**

The finite element package MSC/NASTRAN [13] was used for the analysis. A 2-D finite element model of the complete specimen was created and is shown in fig. 11a. This model was used to determine the stress distribution around the radius and through the thickness for comparison with the closed form solution, and to determine the global variation of G with delamination length. The model used 4-noded isoparametric elements. Around the curved region there was one element per ply thickness and one element per one degree sweep. Larger elements were used in the legs and the arms. The final model had approximately 8100 degrees of freedom. A matrix crack was modeled through the group of $[90]_3$ plies nearest to the smallest radius (R=5mm) at an angle of 45° around the radius. This crack location was consistent with the crack observed experimentally in figs. 9 and 10. Delaminations were modeled emanating in each of the four directions from the matrix crack in one direction at a time, see fig. 11b. The notation for the paths of these cracks is given in fig. 12. To simulate the matrix crack and delamination in the model, a free surface was included by the use of coincident nodes. The coincident nodes were restrained together using multi-point constraints (MPCs). By releasing the appropriate MPCs in different analysis cases, several delamination

lengths could be modeled using one finite element mesh. Strain energy release rate was determined using the virtual crack closure method [14]. This model will be described as model 1.

A full 3-D model of only the curved region was also created. The model is shown in fig. 11b and is referred to as model 2. The model was rigidly supported at one end. Only half the width, w, was modeled because of symmetry. The total width was 25mm. A matrix crack was modeled in the same location as in model 1. To reduce the number of degrees of freedom, only the delamination growing clockwise from the bottom of the matrix crack was modeled, that is, along path b1, see fig. 12. The 2-D model showed that a delamination was most likely to form along this path. Near the matrix crack and the free edge, the elements were 1/16 of a ply thickness square by one ply thickness wide (z-direction), where one ply thickness equals 0.125mm. This refinement was used to capture any G variations in the close vicinity of the matrix crack. The model had approximately 30,000 degrees of freedom and used 6 and 8 noded, solid, modified isoparametric elements. This model was also used to determine the effects of the free edges on the stress distribution assuming an undamaged laminate.

## ANALYTICAL RESULTS

### Stress Analysis

Figure 13 shows the variation of the radial and shear stress and fig. 14 the variation of the tangential stress with $\theta$ in lay-up A. The plots are in the first tension loaded 90° ply as indicated

by the arrow on the figures. The stresses were determined from model 1 and the closed form solution and $\theta$ is defined in fig. 12. In fig. 13 the two solutions agree reasonably well around much of the curved portion and diverge towards $\theta=0^\circ$ and $\theta=90^\circ$ because of the differences in boundary conditions. In fig. 14 the agreement is poor but the trend of the variation with theta is similar. Between $25^\circ<\theta<75^\circ$ the stresses vary by only a small amount and failure might initiate anywhere in this region.

Figure 15 shows the radial and shear stress components plotted across the width along the first 0/90 interface determined using model 2. Also, plotted for comparison, are the results from the closed form solution. Figure 15 shows that the radial stress is largest at the free edge, indicative of the singular nature of the interlaminar radial stress at the free edge in a 0/90 interface. No attempt was made to further refine the finite element mesh at the edges to show more clearly the singular stresses because of the large number of degrees of freedom of the current model. The closed form solution compared well to the FEA solution away from the free edge. The shear stress FEA results in fig. 15 did not agree well with the closed form solution. However the difference is small compared to the magnitude of the radial stress.

Figures 16, 17 and 18 show the variation of the radial, tangential and shear stresses, respectively, through the thickness in lay-up A as determined from model 1, model 2 and the closed form solution and are plotted at $\theta=45^\circ$. The results from model 2 are

plotted at 2z/w=0.0 (the free edge) and 2z/w=1.0 (the center line). In fig. 16 the 2-D FEA results and the closed form solution agree reasonably well for the radial stress. The radial stress reaches a maximum towards the center of the laminate in the 0° plies. At the center line the results compare well with the closed form solution. However, at the free edge the two solutions vary, demonstrating the singular nature of the stresses at the free edge. In fig. 17 the tangential stress reaches a maximum at the inside edge, $(R-R_{inner}/t=0.0)$ where there is a 0° ply. For the 90° plies, the tangential stress has a maximum tension value in the 90° ply closest to the inner radius, $(R-R_{inner}/t)=0.167$. The tangential stress at this location may contribute to matrix cracking in these plies. The results for all three solutions agree reasonably well. In fig. 18, the shear stress results from the closed form solution and the 2-D FEA solution agree well, and the shear stress is small. From the 3-D solution in the center, the results are inconsistent with the 2-D solutions. The cause for this is not known presently but may be caused by the large aspect ratio of the elements in the center width of the model.

**Strain Energy Release Rate Analysis**

In ref. 6 the variation in G with delamination length for delamination growth from a matrix crack along each of the four paths shown in fig. 12, was determined for lay-up B. The value of G along path b1, $G_{b1}$, was usually higher than the other three values ($G_{a1}$, $G_{a2}$ and $G_{b2}$), fig. 19. Therefore, it was assumed

delamination would initiate along path b1. In ref. 4 a technique for predicting the delamination growth path for a delamination with two fronts was given. The technique consisted of comparing the values of G at each front and growing the delamination at the location of the highest G. Following a similar method the next highest value to $G_{b1}$ was $G_{a2}$. By assuming growth along b1 and comparing values of $G_{a2}$ to $G_{b1}$ it was observed that $G_{b1}$ was always larger than $G_{a2}$ around most of the curved portion. Therefore, delamination should grow along the b1 path followed by delamination along path a2 as observed in fig. 10. Figure 20 shows the variation of $G_{b1}$ with $\beta$ for lay-up B. Because $G_{b1}$ is continually increasing, delamination growth should be unstable once initiated as observed experimentally. Also, shown in fig. 20 is the mode I component of strain energy release rate, $G_I$. Because of the oscillatory nature of the stress fields between plies of different orientation the mode I value may not converge [15]. However, with the element size used, the delamination remained largely mode I around much of the curved portion due to the high radial stresses present. The above analyses were not repeated for lay-up A. A similar result is expected since the matrix crack and delamination paths in figs. 9 and 10 are similar.

Figure 21 shows the distribution of $G_{b1}$ across the width at several delamination lengths (angle $\beta$) from the matrix crack for lay-up A using model 2. Across 80 percent of the width G was constant and reached a maximum at the free edge. The results are

very similar for lay-up B in ref. 6. Figure 21 indicates that the delamination front may not remain straight and perpendicular to the edge as it grows. Delamination front curvature was not considered in the analysis. Figure 22 shows the variation of G with $\beta$ using model 2. As delamination grows, the rate of change of G initially decreases and then begins to increase with a point of inflection in between. Close to the matrix crack G is very small. Also shown in fig. 22 are the results using model 1 (solid circular symbols). As expected, the values of G from model 2 in the interior are similar to those obtained from the 2-D model. A polynomial curve fit expression to the G distribution on the free edge and the center line is shown in fig. 23. The first part of this curve, where $dG/d\beta$ is decreasing, may be analogous to the distributions for edge delamination [2], fig. 2a or for delamination from dropped plies [3], fig. 2b where the singular stress source, the edge and the dropped ply, respectively, dominates the G distribution. However, for the curved laminate, there is a high radial force which also contributes to G and causes $dG/d\beta$ to increase with no peak or plateau as observed in refs. 2 and 3. It was postulated in ref. 6 that the point of inflection may be used to determine a critical value of G to predict delamination growth much as the plateau or peak value in refs. 2 and 3. At the free edge in lay-up A, the point of inflection ($d^2G/d\beta^2=0$) was determined to be at $\beta=2.13^\circ$ (1.6 ply thicknesses from the matrix crack) yielding a critical value of ($G\ w^2/P^2$) = 8.08E-4 mm/N. At the center of the width the point of

inflection was determined to be at $\beta$=1.08° (0.83 ply thicknesses from the matrix crack) yielding a critical value of ($G\ w^2/P^2$) = 4.17E-4 mm/N. These values of G may be compared to the static and fatigue toughness of the composite to predict delamination onset for the curved laminate.

## DAMAGE ONSET PREDICTIONS

### Delamination from Radial Stresses

In refs. 16 and 17 delamination was predicted by comparing the maximum radial stress to the transverse strength of the composite. If the delamination occurs in a 0/90 interface and the analysis used to determine the maximum radial stress ignores the effects of the free edge, this prediction technique may be incorrect and any correlation between experimental failure loads and predictions may be coincidental. However, if the delamination occurs between plies of the same orientation then this technique is valid. Figure 9 shows an interlaminar tension failure in the 0° plies as well as a matrix crack with delaminations emanating from it. It is not known which occurred first. From the closed form solution in fig. 16 the maximum normalized radial stress in the 0° plies was ($\sigma_r$ w/P) = 4.04 $mm^{-1}$ at ($R-R_{inner}/t$)≈0.42. At this location the tangential and shear stresses were negligible. By comparing this value of radial stress to the interlaminar tensile strength results shown in fig. 6, a prediction for lay-up A can be made using eq. 3 and is shown in fig. 24. Individual experimental data points from fig. 6 have been used for the predictions. The predictions are

$$\frac{P_{max}}{w} = \frac{\sigma_{3max}}{\left(\frac{\sigma_r w}{P}\right)} = \frac{\sigma_{3max}}{4.04} \qquad (3)$$

close to the experimental failures and are slightly conservative. From fig. 10 no interlaminar tension delaminations occurred alone in lay-up B and the criterion in eq. 3 is not relevant.

**Transverse Ply Cracking Prediction**

A strength based failure criterion could possibly be used to predict the onset of matrix cracking in the 90° plies. However, the 3-D stress analysis showed the presence of stress singularities at the free edge. Also, the strength of the composite in the 90° flat tension specimens may not be the same as the in-situ strength of the 90° plies in the laminate [18]. Therefore, any predictions must be purely qualitative and are included in this paper to show that matrix cracking in the 90° plies may occur. In the 90° plies there is a biaxial stress state composed of the radial and tangential stresses. The Tsai-Hill criterion has been derived for predicting first ply failure in composite lamina [19] as

$$\frac{\sigma_{11}^2 - \sigma_{11}\,\sigma_{22}}{X^2} + \frac{\sigma_{22}^2}{Y^2} + \frac{\tau_{12}^2}{S^2} = 1 \qquad (4)$$

where X, Y are the tensile strengths in the 1 and 2 directions and S is the 12 shear strength. In the curved laminates the shear ratio is negligible compared to the radial and tangential ratios and may be neglected in eq. 4. Re-writing eq. 4 in terms of the

normalized radial and tangential stresses and omitting the shear stress terms, a predicted load per unit width may be determined as

$$\left(\frac{w}{P_{max}}\right)^2 = \frac{\left(\frac{\sigma_r w}{P}\right)^2 - \left(\frac{\sigma_r w}{P}\right)\left(\frac{\sigma_\theta w}{P}\right)}{(\sigma_{3max})^2} + \frac{\left(\frac{\sigma_\theta w}{P}\right)^2}{(\sigma_{2max})^2} \qquad (5)$$

From the closed form solutions in figs. 16 and 17 the maximum radial and tangential stresses were $(\sigma_r \ w/P) = 3.91 mm^{-1}$ and $(\sigma_\theta \ w/P) = 2.35 \ mm^{-1}$, respectively. Because individual data points may not be used in eq. 5 for $\sigma_{2max}$ and $\sigma_{3max}$, straight line lower and upper bound curves were fit to the transverse tension and interlaminar tension fatigue data in figs. 3 and 6, respectively. These curves were drawn for demonstration purposes only and are not meant to characterize the material property. Using these straight line fits in eq. 5 lower and upper bound predictions can be made and are shown in fig. 25. The prediction curves indicate that matrix cracking may occur prior to final failure of the curved laminate. These prediction curves do not take into account the singular nature of the stresses at the free edge nor the residual thermal stresses both of which will effectively reduce the fatigue life further. Also, as mentioned in the experimental work, some of the 90° flat specimens failed in the grips and hence may under estimate the transverse strength of the composite.

**Delamination Onset from the Matrix Crack**

If a matrix crack is assumed to already exist, the values of G calculated at the point of inflection may be compared to the

delamination data obtained from the DCB in fig. 7. The G distribution in fig. 20 showed that delamination was predominantly mode I. If the G distribution had significant mode II and III components a mixed mode failure criterion would be necessary. However, assuming a total G criterion and comparing it to mode I data will yield a conservative approach [3,5,10]. A predicted load per unit width may be determined from eq. 6.

$$\frac{P_{max}}{w} = \sqrt{\frac{G_{Imax}}{\left(\frac{G\ w^2}{P^2}\right)}} \qquad (6)$$

The results of this prediction are shown in fig. 26 using the values of normalized G at the free edge and in the center. The predictions at the free edge are conservative and the predictions at the center are close to the experimental data. This prediction does not include the number of cycles to form the matrix crack and hence will generally be a conservative prediction. In the analysis the matrix crack was assumed to be straight; it is not clear how an angled crack would effect the G distribution or the mode I/mode II mix of G. However, if a mode II component was present it would be anticipated that the predicted number of cycles to delamination onset would be higher because of the higher fatigue and fracture toughness in mode II [10]. It is probable that the matrix crack occurred before the delamination although it was not detected prior to final failure in the experimental work.

## DISCUSSION

If the stresses that cause delamination are not singular, then damage onset or delamination may be predicted using a strength criterion. This was demonstrated for interlaminar tension delaminations initiating in the 0° plies. However, if the stresses are singular, such as at a free edge or a discontinuity, a fracture mechanics prediction technique represents a means for predicting damage onset and growth. This was demonstrated for delaminations initiating from a matrix crack. Because closed form and 2-D FEA solutions do not account for free edge singularities, strength predictions may be inaccurate and more importantly potentially unconservative using these analyses techniques. Therefore, it is important to determine where damage initiates before selecting a particular criterion to predict it. However, 2-D analyses are useful for initial design because damage initiation depends on lay-up. For example, matrix cracks can be avoided if a lay-up is chosen so that the tangential stresses in the 90° plies are not highly tensile. Also, free edge delamination may be minimized if a lay-up is chosen so that the radial stresses are low at 0/90 interfaces (or other perpendicular interfaces e.g. +45/-45).

Because of matrix cracking and interface effects at free edges multidirectional laminates should not be used to determine interlaminar tensile strength, $\sigma_{3c}$ unless it is certain that interlaminar tension failure occurs within a group of plies of the same orientation. The simplest means to ensure this is in a

unidirectional curved beam [4]. In ref. 4 a 2-D closed form analysis of a unidirectional curved laminate determined that the stresses were purely radial at the failure location in the laminate.

## SUMMARY

This paper details the analytical and experimental work required to predict delamination onset in a curved composite laminate subjected to static and fatigue loads. The composite used was AS4/3501-6, graphite/epoxy. Analytically, a closed form stress analysis and a 2-D and a 3-D finite element analyses were conducted to determine the stress distribution in an undamaged curved laminate. The finite element analyses were also used to determine values of strain energy release rate at a delamination emanating from a matrix crack in a 90° ply. Experimentally, transverse tensile strength and fatigue life were determined from flat 90° coupons. The interlaminar tensile strength and fatigue life were determined from unidirectional curved laminates. Also, mode I fatigue and fracture toughness data were determined from double cantilever beam specimens. The analysis and the strength and toughness data were used to predict the static and fatigue strength of cross-plied curved laminates. The prediction for interlaminar tension delamination in the 0° plies was in reasonable agreement with the experimental results for the curved laminate. The interlaminar fracture mechanics approach compared the critical value of strain energy release rate at the free edge, and in the

center, to the fatigue and fracture toughness of the composite. The predictions at the free edge were conservative and the predictions at the center were in agreement with the experimental data. This prediction does not include the number of cycles to form the matrix crack and hence will generally be a conservative prediction.

## REFERENCES


1. Kedward, K.T., Wilson, R.S., and McLean, S.K., "Flexure of Simply Curved Composite Shapes," Composites, Vol. 20, No. 6, November 1989, pp. 527-536.

2. O'Brien, T.K., "Mixed-Mode Strain-Energy-Release Rate Effects on Edge Delamination of Composites," Effects of Defects in Composite Materials, ASTM STP 836, D.J. Wilkins, Ed., American Society for Testing and Materials, Philadelphia, 1984, pp. 125-142.

3. Murri, G.B., Salpekar, S.A., and O'Brien, T.K., "Fatigue Delamination Onset Prediction in Tapered Composite Laminates, "to appear in Composite Materials: Fatigue and Fracture (3rd Volume), ASTM STP 1110, T.K. O'Brien, Ed., 1991. Also published as NASA TM 101673, December 1989.

4. Martin, R.H., "Delamination Failure in a Unidirectional Curved Composite Laminate,' presented at the 10th ASTM Symposium on Composite Materials: Testing and Design, San Francisco, April, 1990. Also published as NASA CR 182018, April 1990.

5. O'Brien, T.K., "Local Delamination in Laminates with Angle Ply Matrix Cracks: Part II - Delamination Analysis and Characterization," to be presented at the 4th ASTM Symposium on Composite Materials: Fatigue and Fracture, Indianapolis, May 6-7, 1991. Also published as NASA TM 104076, 1991.

6. Martin, R.H., "Analysis of Delamination Onset and Growth in Curved Laminates," to be presented at the 8th ASCE Engineering Mechanics Speciality Conference, Ohio State University, Columbus, Ohio, May 19-22, 1991.

7. Salpekar, S.A., and O'Brien, T.K., "Combined Effect of Matrix Cracking and Stress-Free Edge on Delamination," to be published in Composite Materials: Fatigue and Fracture (3rd Volume), ASTM STP 1110, T.K. O'Brien, Ed., American Society for Testing and Materials, Philadelphia, 1991.

8. Sun, C.T., and Kelly, S.R., "Failure in Composite Angle Structures - Part II: Onset of Delamination," Journal of Reinforced Plastics and Composites, Vol. 7, May 1988, pp. 233-244.

9. Paul, P.C., Saff, C.R., Sanger, K.B., Mahler, M.A., Kan, H.P., and Kautz, E.F., "Analysis and Test Techniques for Composite Structures Subjected to Out of Plane Loads," presented at the 10th ASTM Symposium on Composite Materials: Testing and Design, San Francisco, April, 1990.

10. Murri, G.B., and Martin R.H., "Effect of Initial Delamination on Mode I and Mode II Interlaminar Fracture Toughness and Fatigue Fracture Threshold," to be presented at the 4th ASTM Symposium on Composite Materials: Fatigue and Fracture, Indianapolis, Indiana, May 6-9, 1991.

11. Martin, R.H., and O'Brien, T.K., "Characterizing Mode I Fatigue Delamination of Composite Materials," Proceedings of the American Society for Composites, Fourth Technical Conference, Blacksburg, Virginia, October 1989, pp. 257-266.

12. Ko, W.L. and Jackson, R.H., "Multilayer Theory for Delamination Analysis of a Composite Curved Bar Subjected to End Forces and End Moments," Composite Structures 5: Proceedings of the 5th International Conference, Paisley, Scotland, July 24-26, 1989, pp. 173-198.

13. NASTRAN Users Manual, Version 66B, MacNeal-Schwendler Corporation, Los Angeles, November 1989.

14. Shivakumar, K.N., Tan, P.W., and Newman, J.C., Jr., "A Virtual Crack-Closure Technique for Calculating Stress Intensity Factors for Cracked Three Dimensional Bodies," International Journal of Fracture, Vol. 36, 1988, pp. R43-R50.

15. Sun, C.T., and Jih, C.J., "On the Strain Energy Release Rates for Interfacial Cracks in Bi-Material Media," Engineering Fracture Mechanics, 28:13-27, 1987.

16. Chang, F.K., and Springer, G.S., "The Strengths of Fiber Reinforced Composite Bends," Journal of Composite Materials, Vol. 20, January 1986, pp. 30-45.

17. Sun, C.T., and Kelly, S.R., "Failure in Composite Angle Structures Part I: Initial Failure," Journal of Reinforced Plastics and Composites, Vol. 7, May 1988, pp. 220-232.

18. Hart-Smith, L.J., "Some Observations About Test Specimens and Structural Analysis for Fibrous Composites," Composite Materials: Testing and Design (Ninth Volume), ASTM STP 1059, S.P. Garbo, Ed., American Society for Testing and Materials, Philadelphia, 1990, pp. 86-120.

19. Tsai, S.W., "Strength Theories of Filamentary Structures" Fundamental Aspects of Fiber Reinforced Plastic Composites, R.T. Schwartz and H.S. Schwartz, Eds., Wiley Interscience, New York, pp. 3-11, 1968.

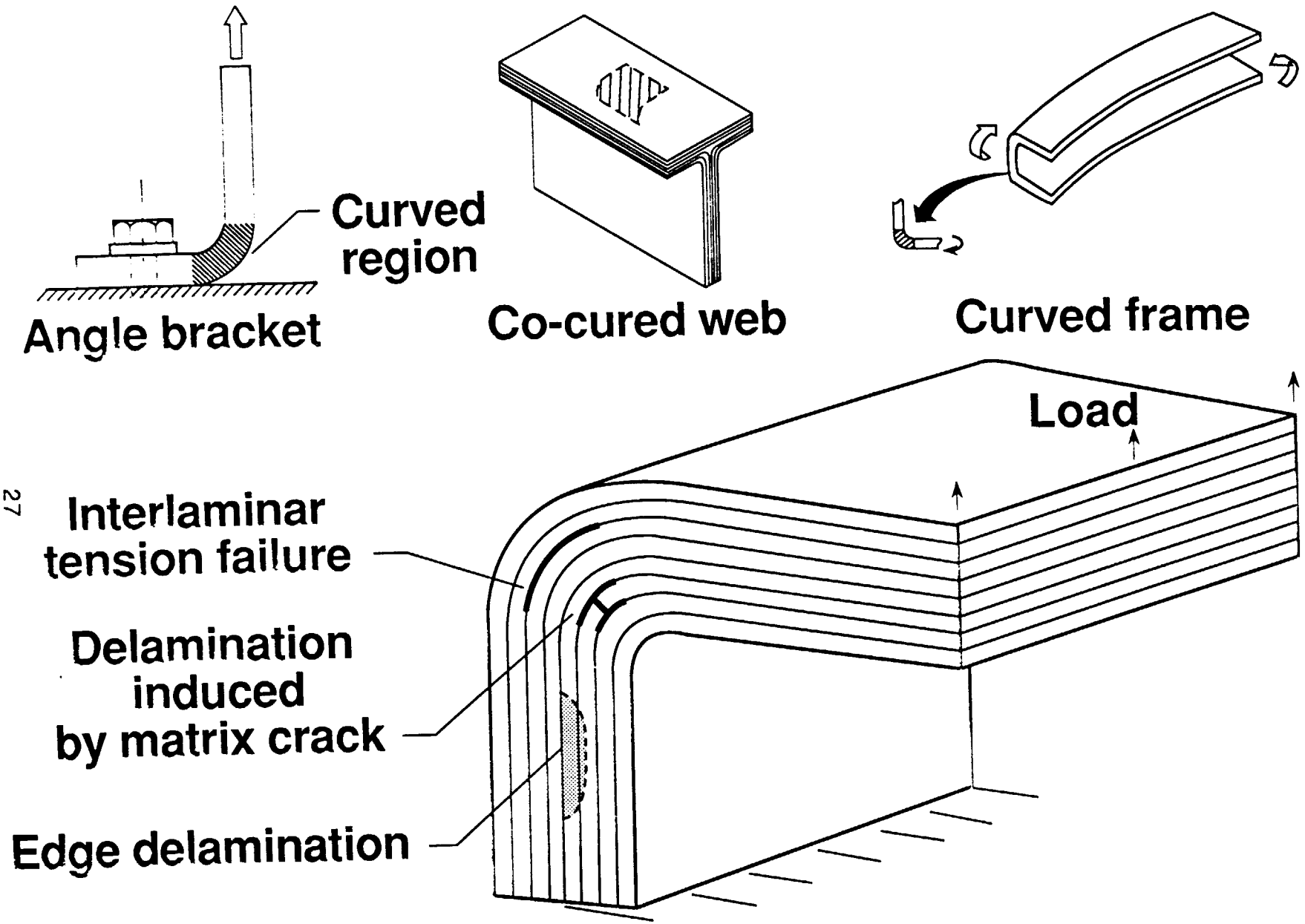


Fig. 1. - Structural configurations and damage modes for curved laminates.

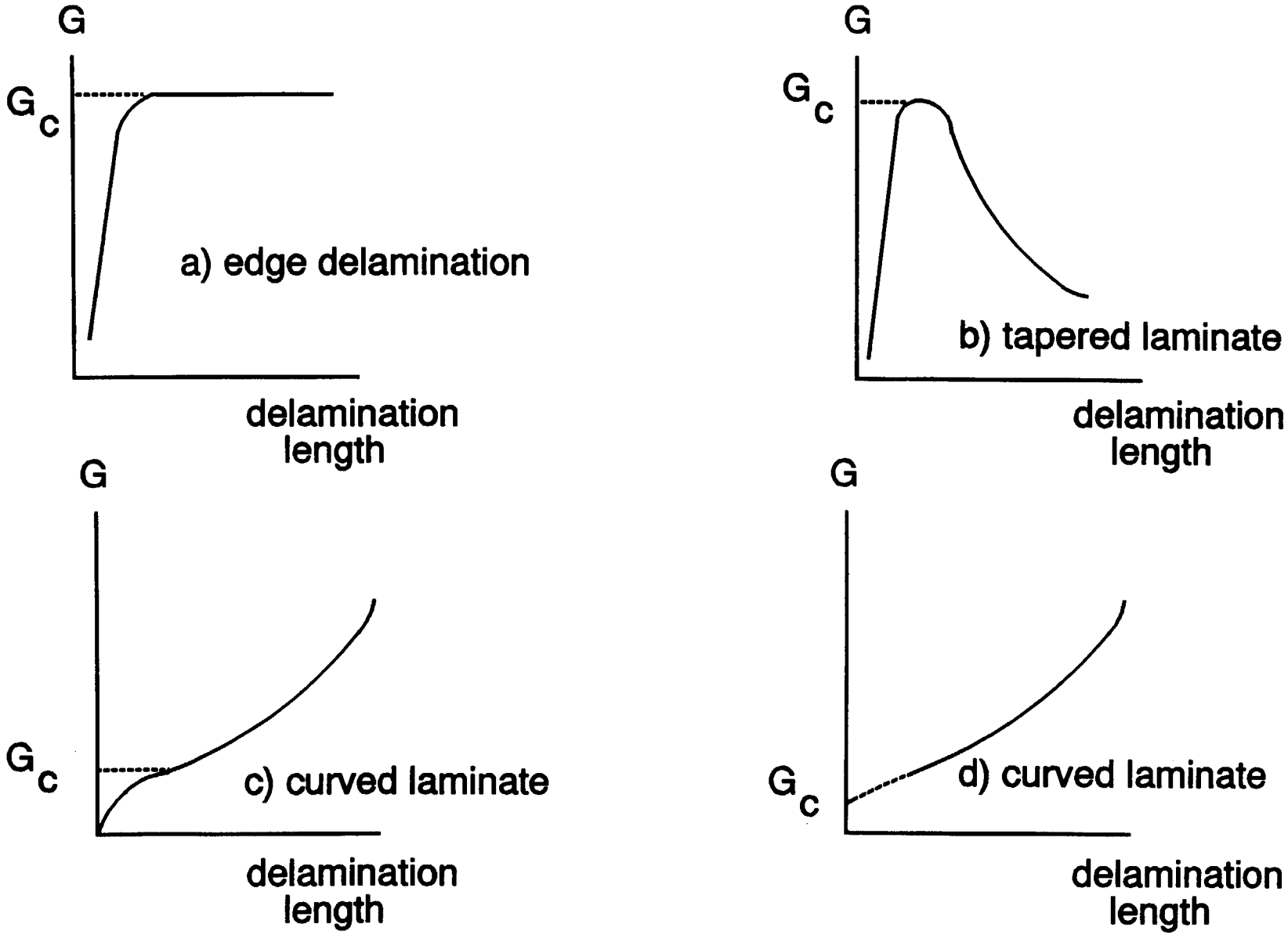


Fig. 2. - Shapes of G curves for different geometries.

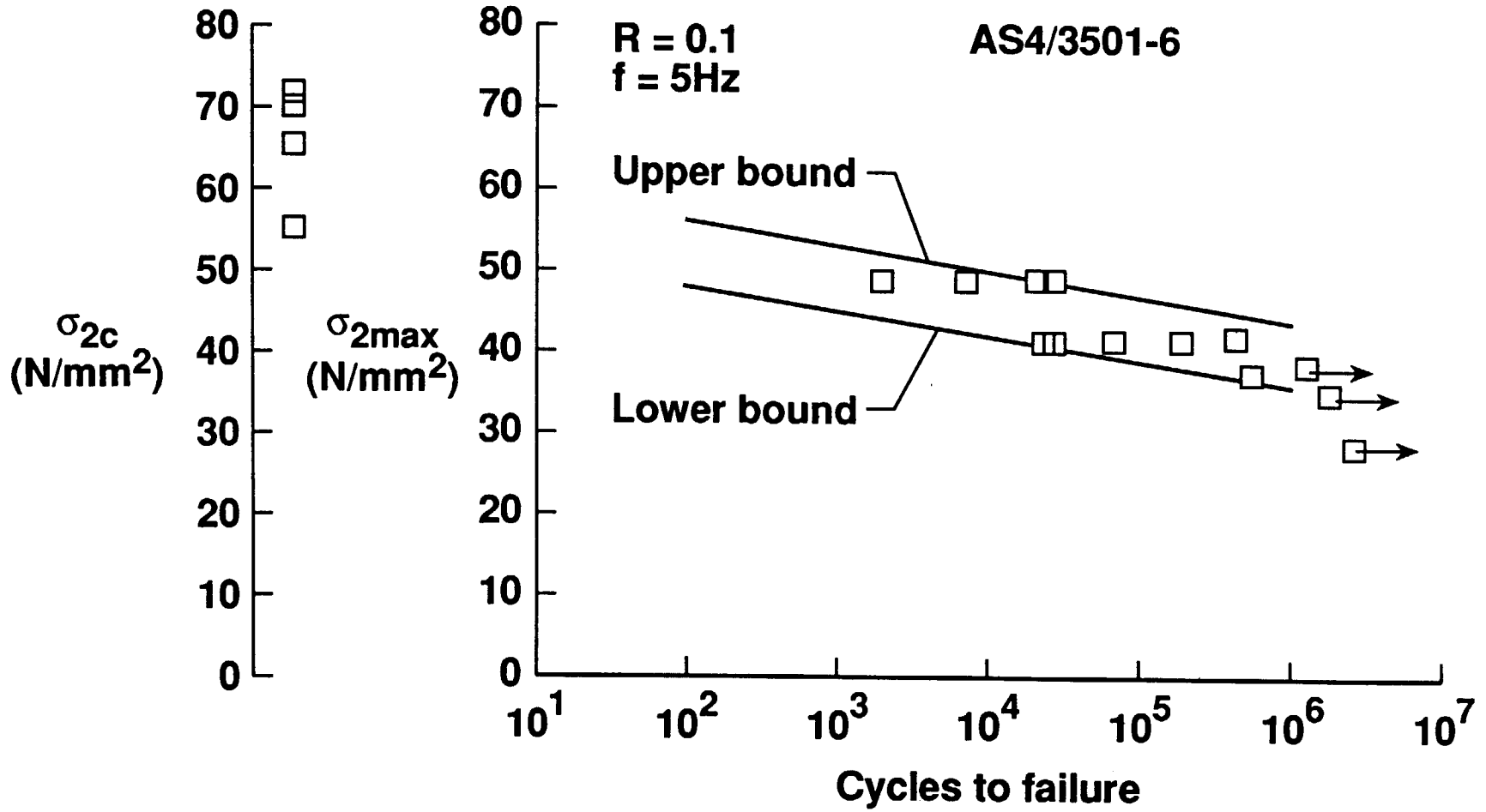


Fig. 3. - Transverse tension static and fatigue strength of AS4/3501-6 from 90° flat laminates.

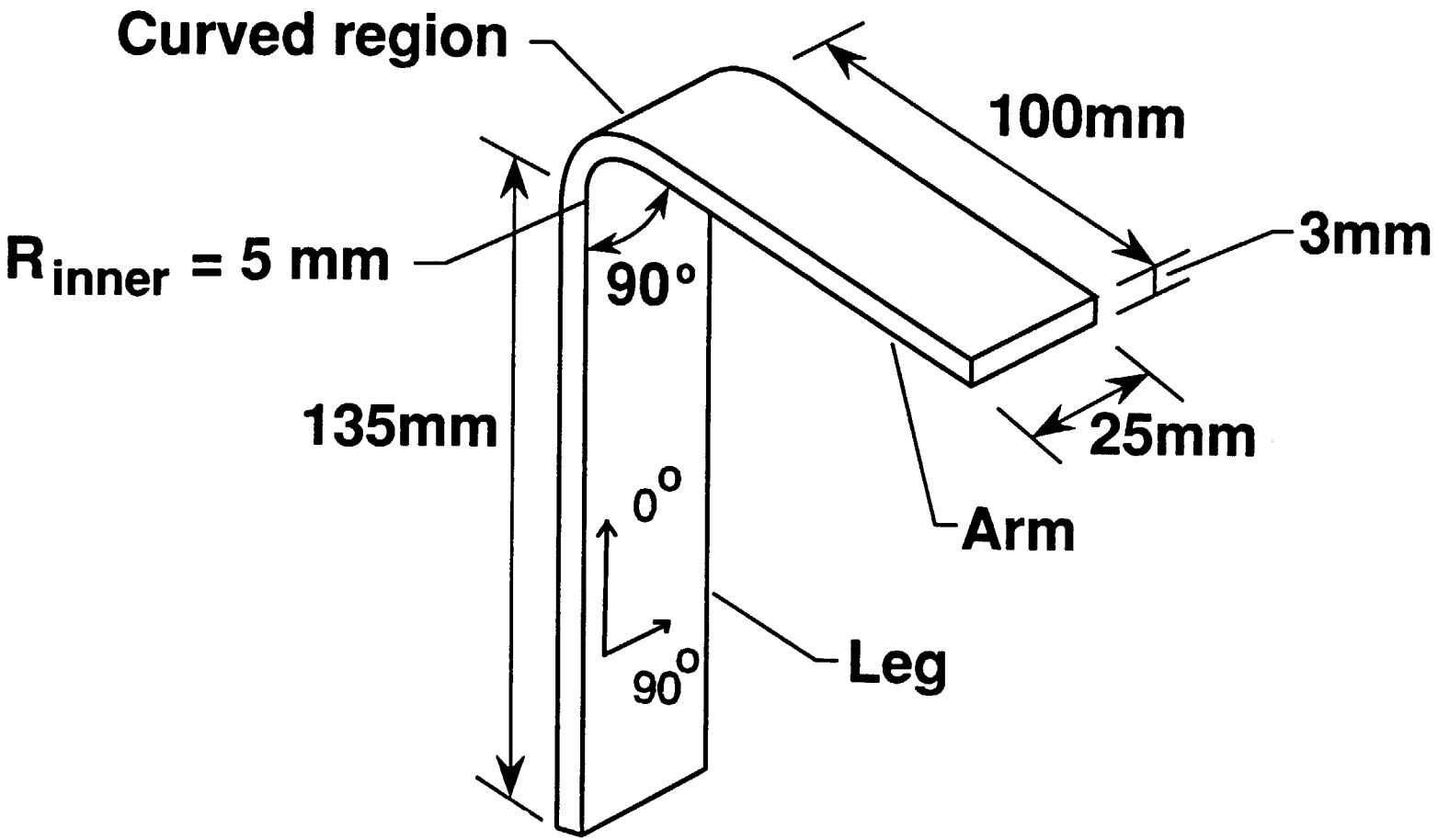


Fig. 4. - Unidirectional and cross plied curved laminate configuration.

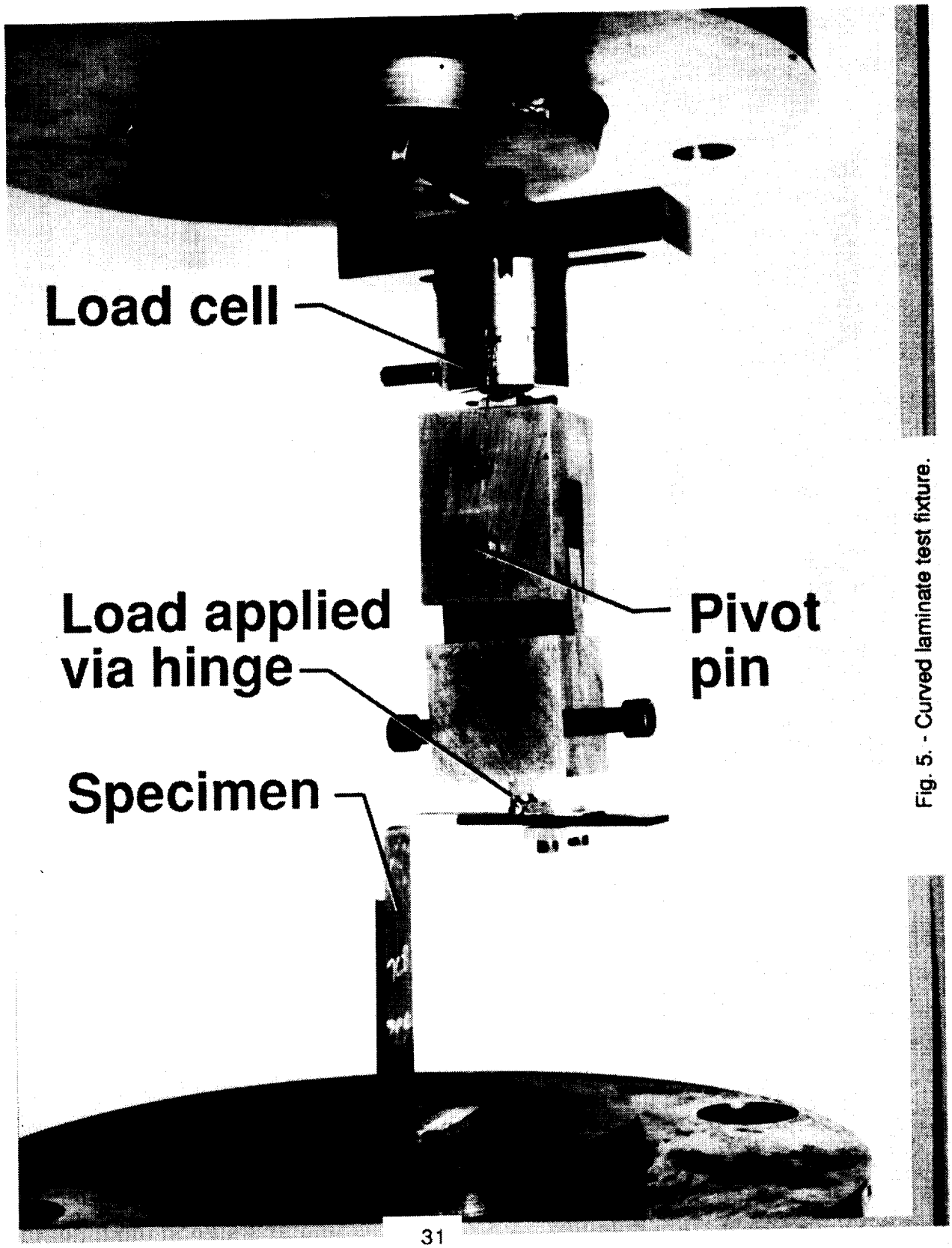


Fig. 5. - Curved laminate test fixture.

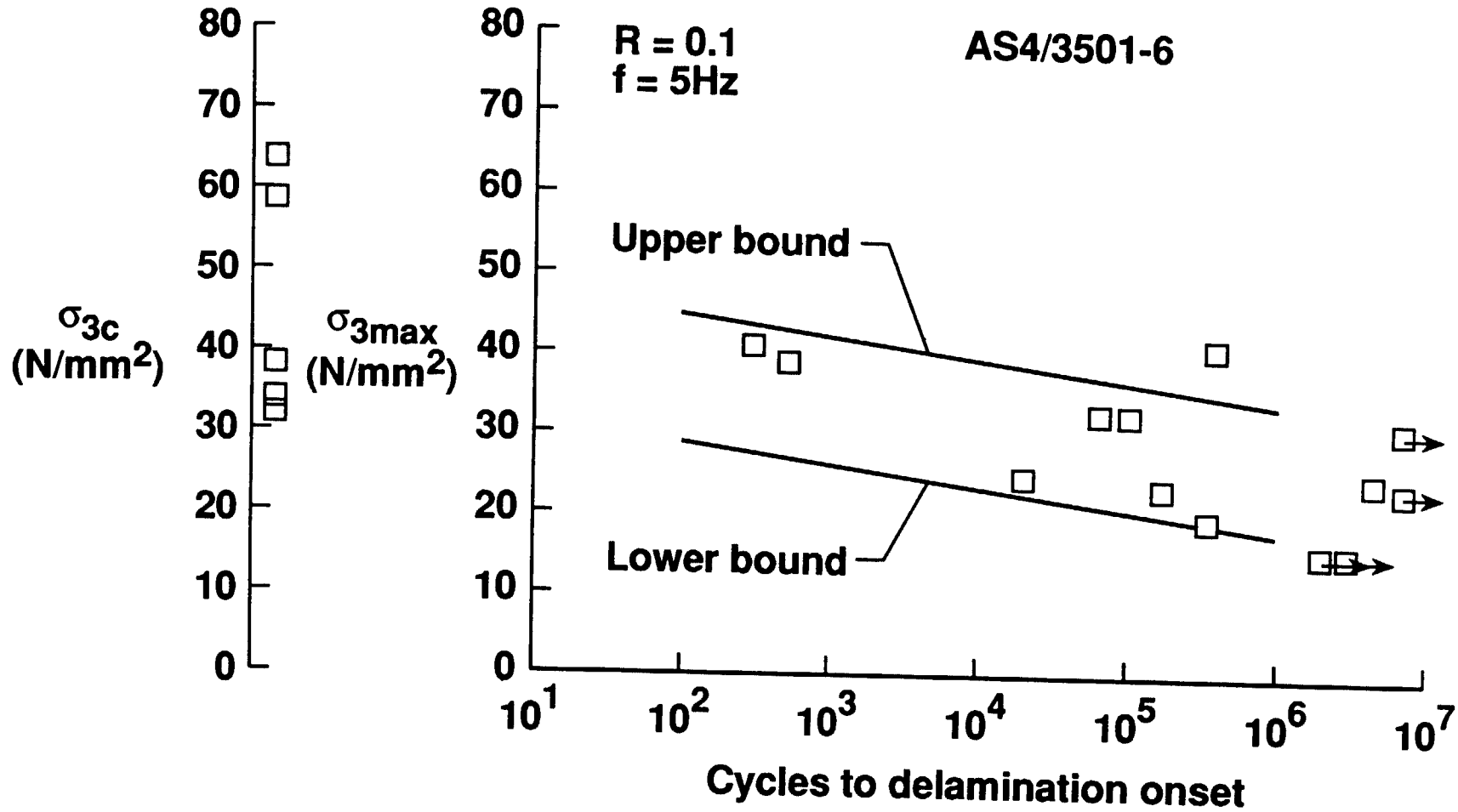


Fig. 6. - Interlaminar tension static and fatigue strength of AS4/3601-6 from unidirectional curved laminates.

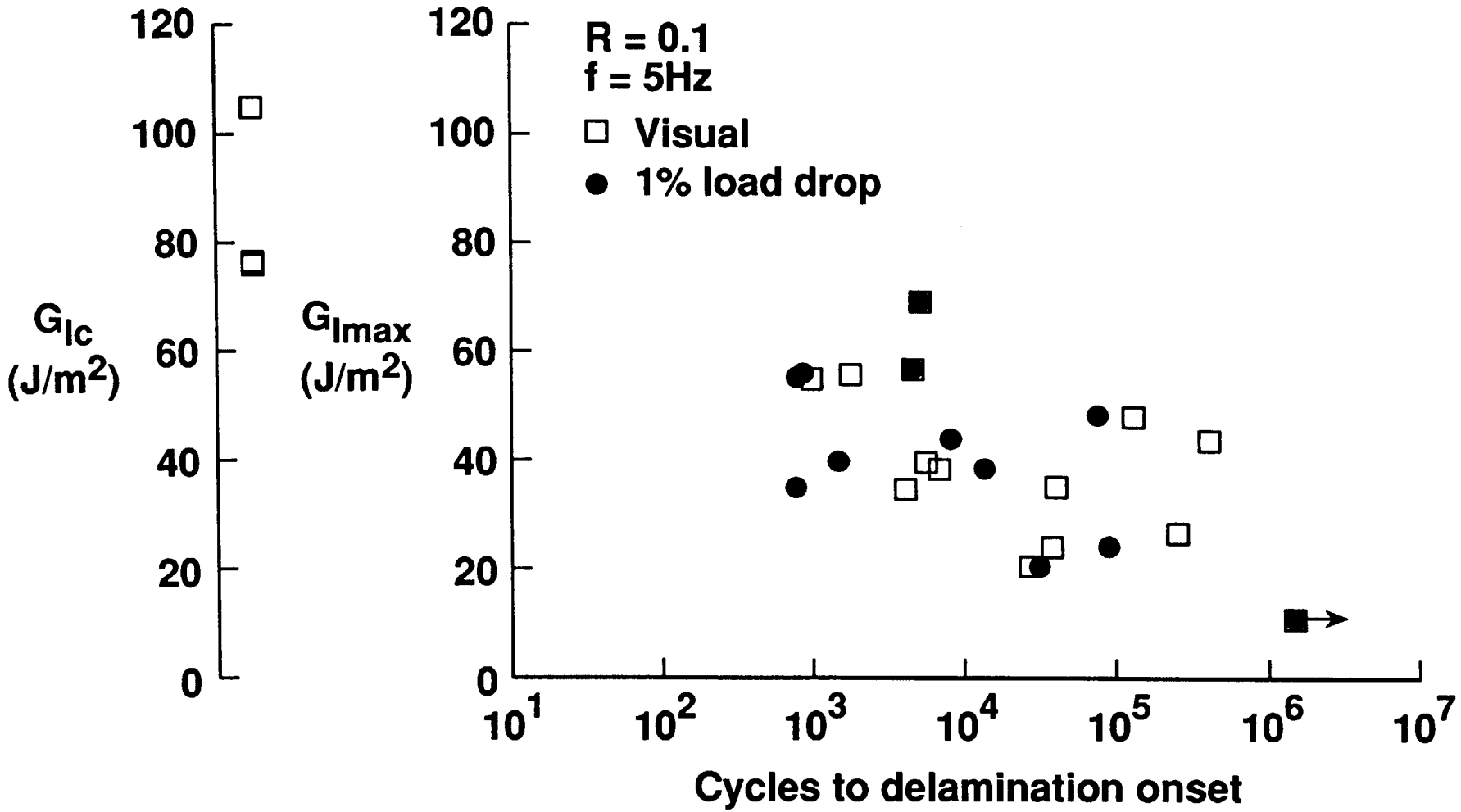


Fig. 7. - Interlaminar static and fatigue fracture toughness of AS4/3501-6 using the DCB specimen.

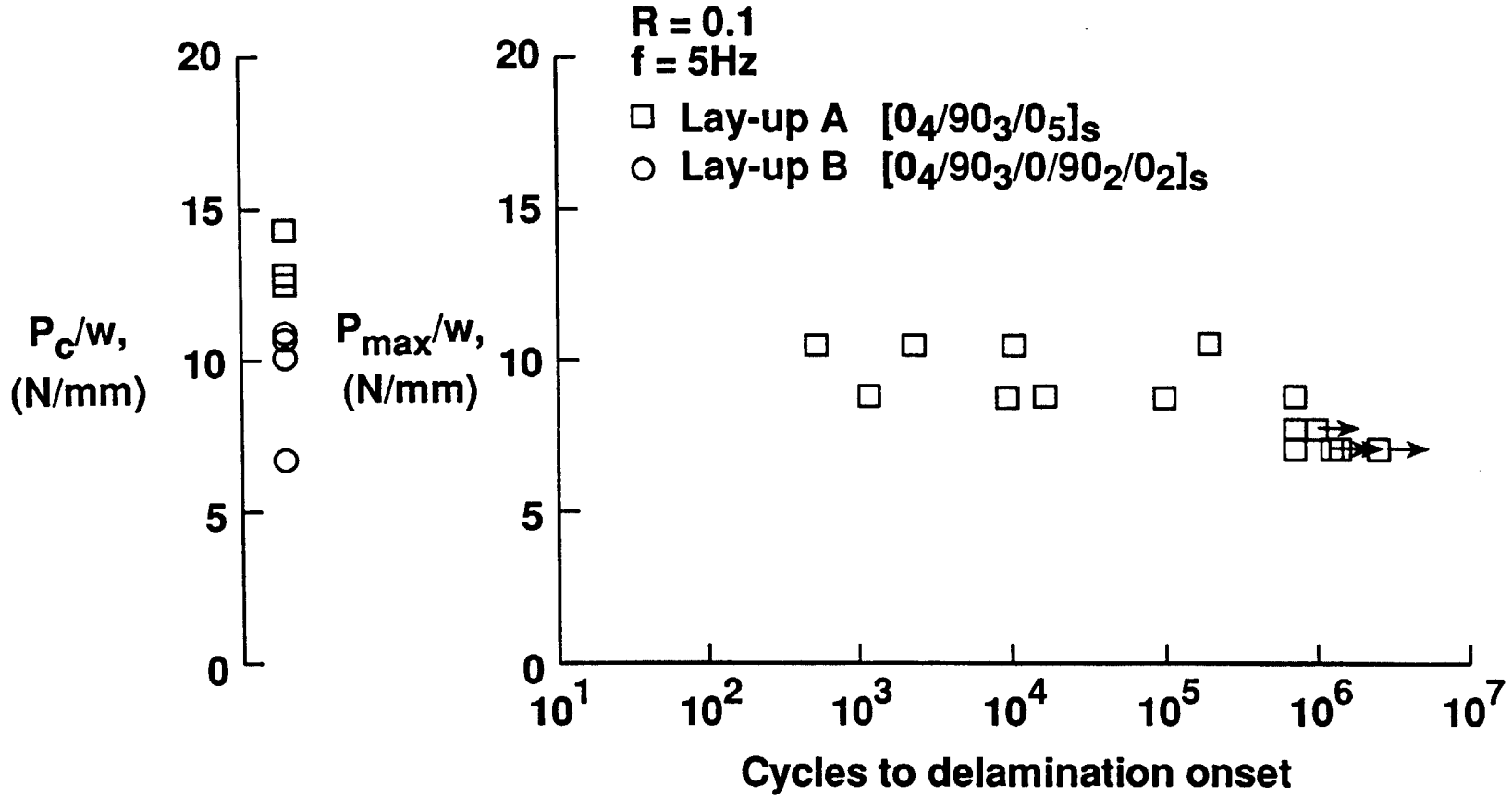


Fig. 8. - Static and fatigue strength of cross plied curved laminates.

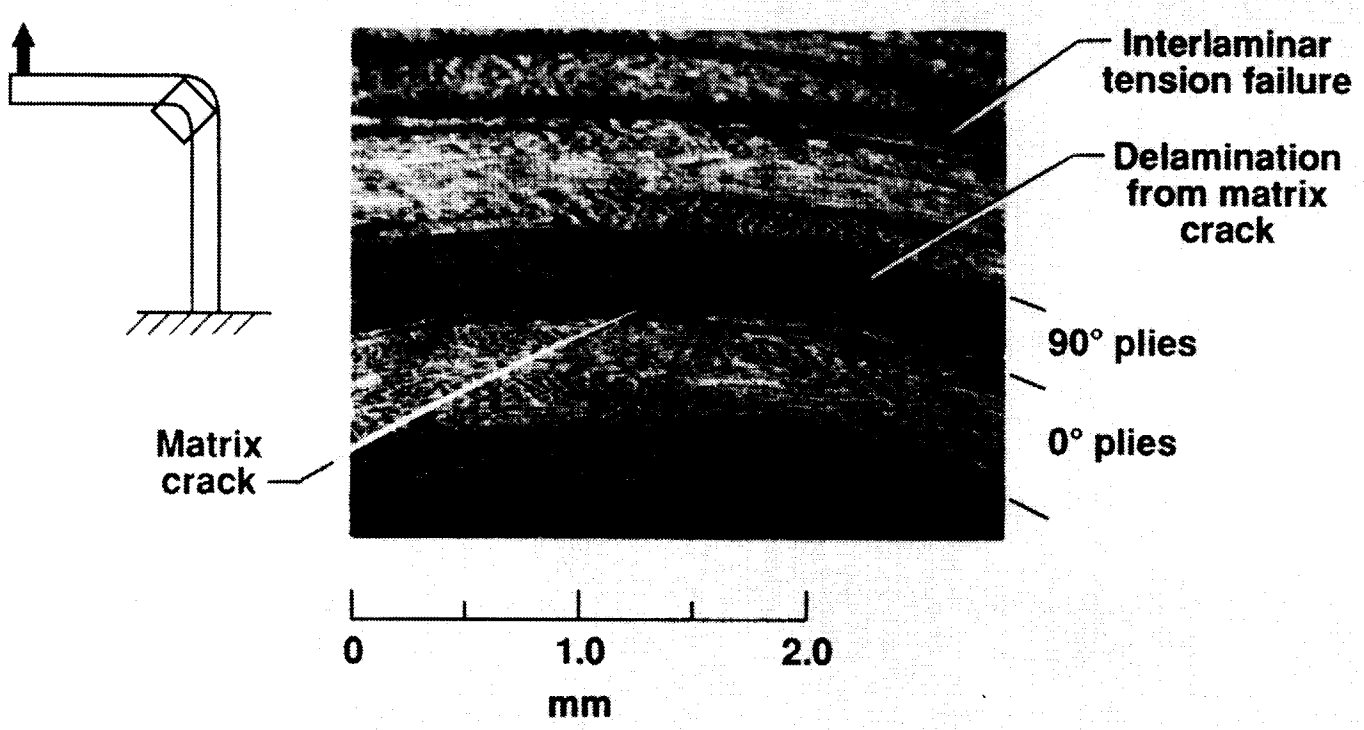


Fig. 9. - Damage in curved laminate - lay-up A.

Fig. 10. - Damage in curved laminate - lay-up B.

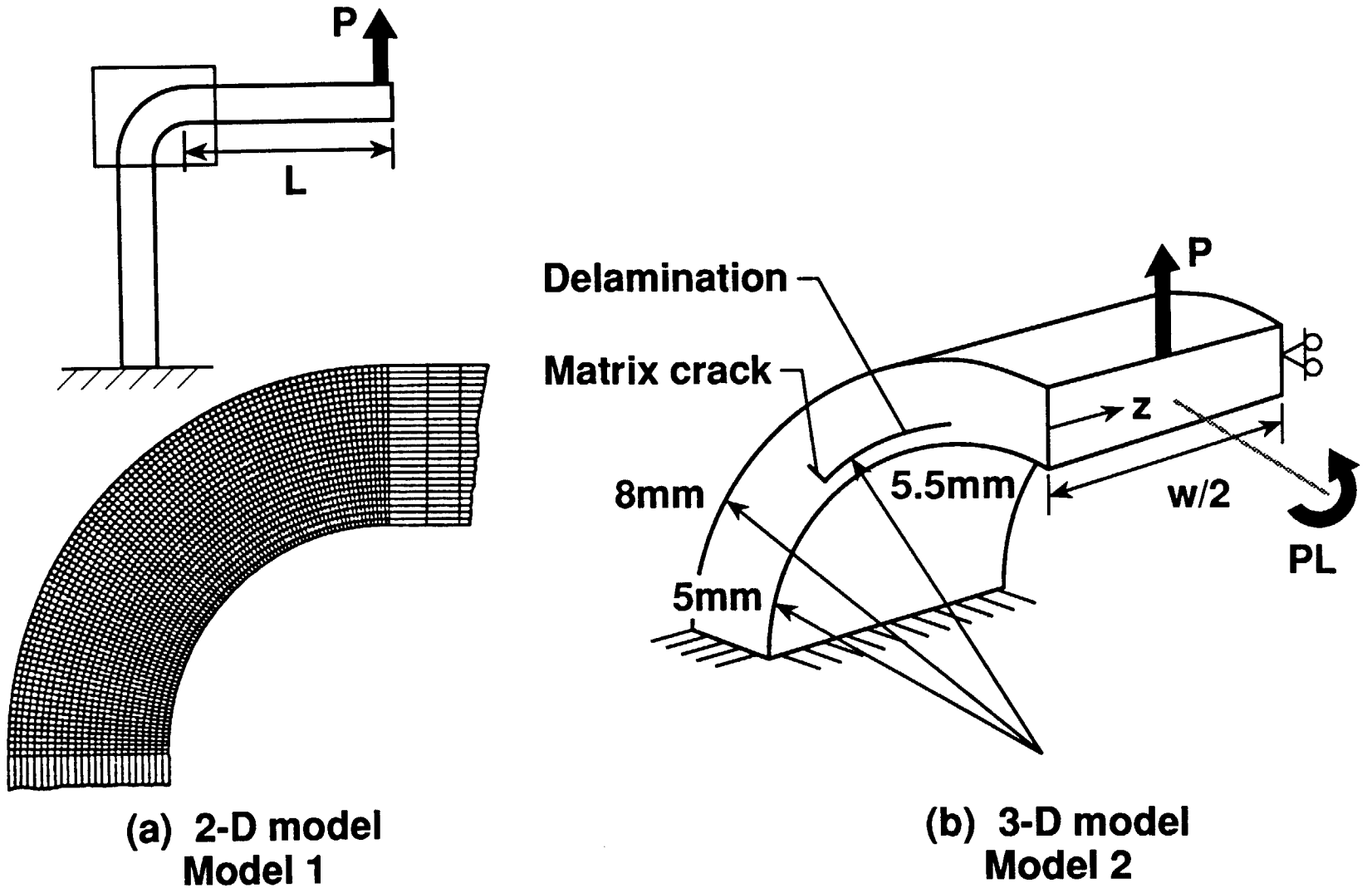


Fig. 11. - Models used in finite element analyses.

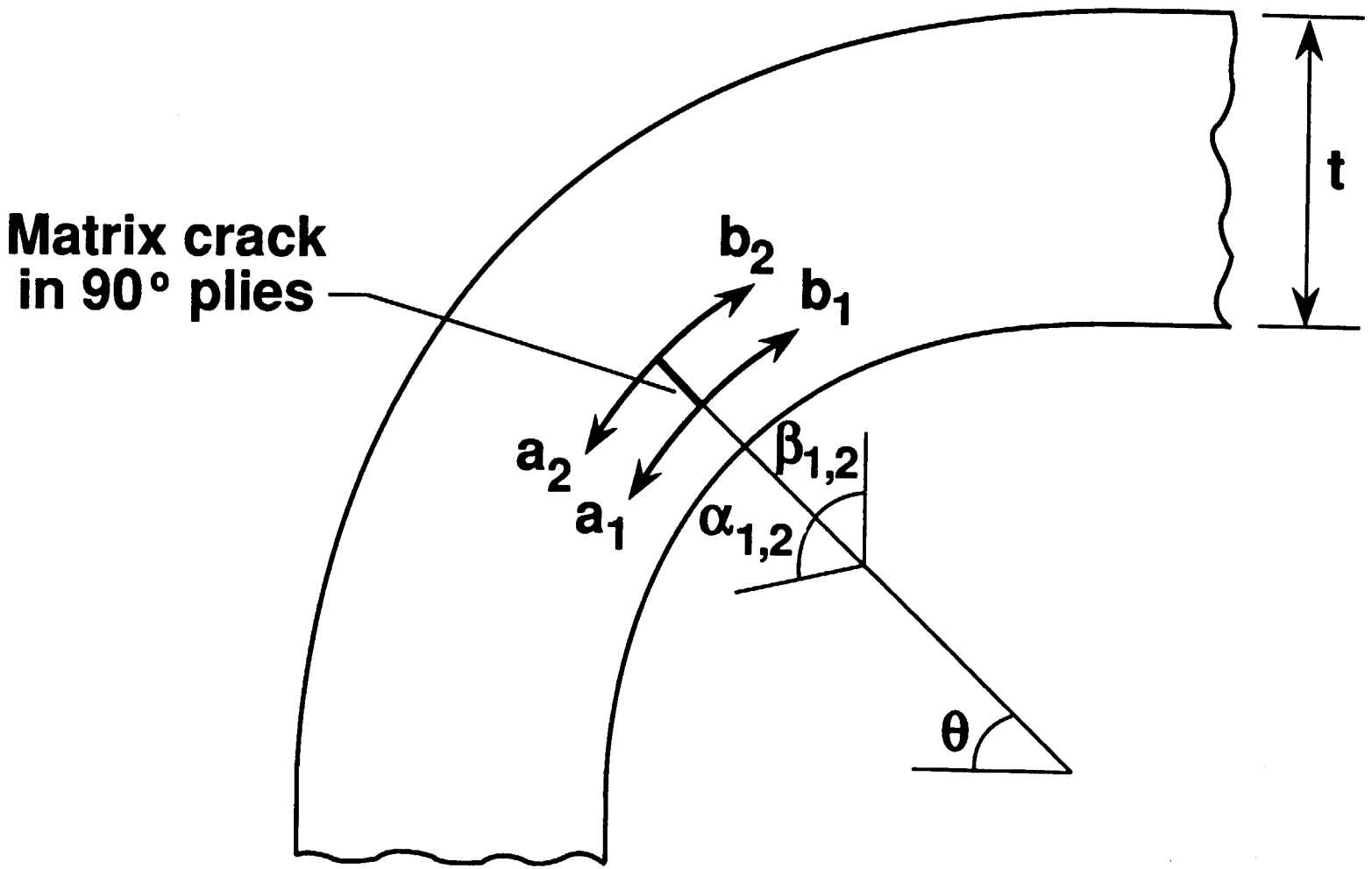


Fig. 12. - Notation for delamination growth from matrix crack.

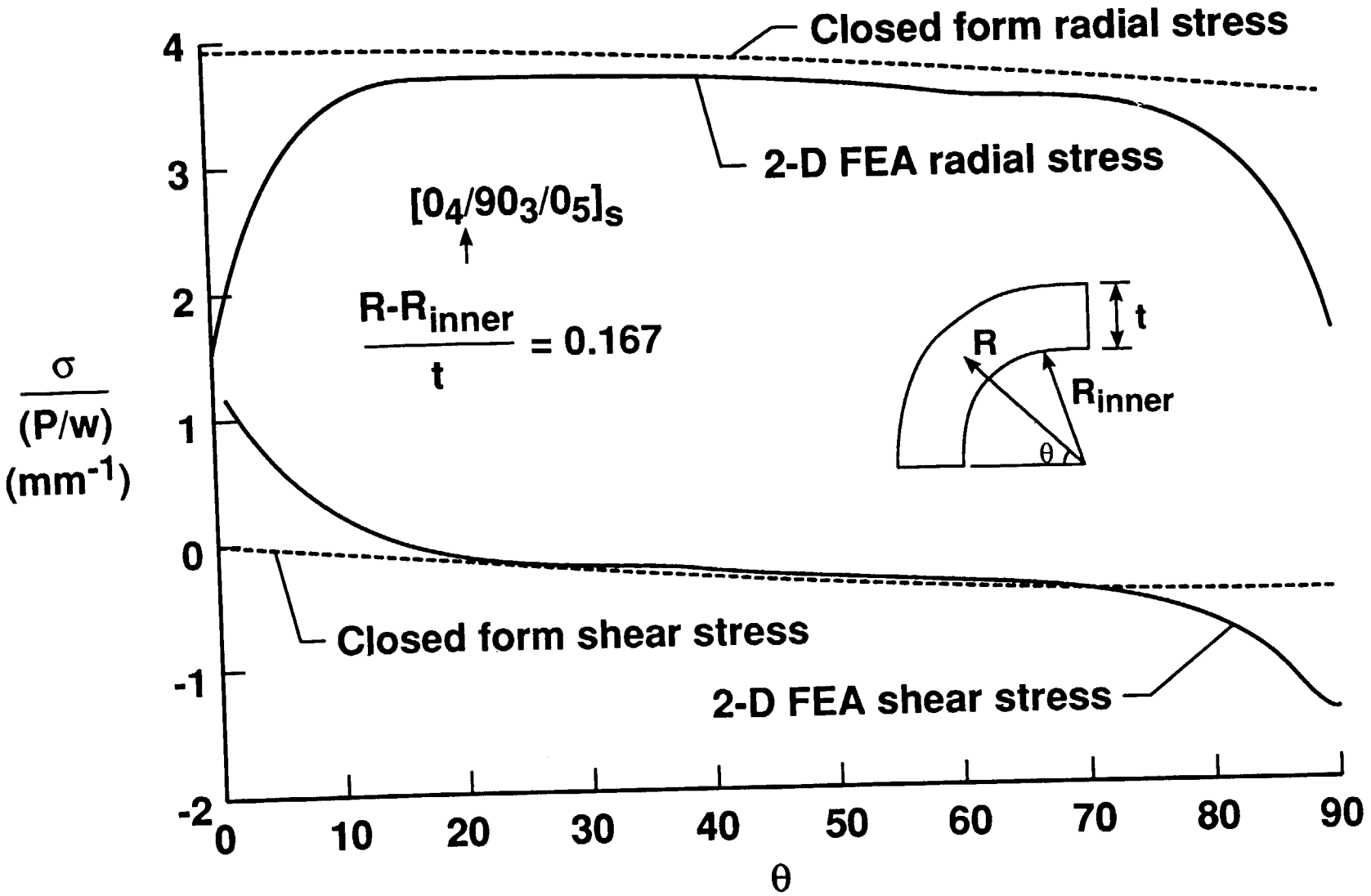


Fig. 13. - Radial and shear stress variation with theta.

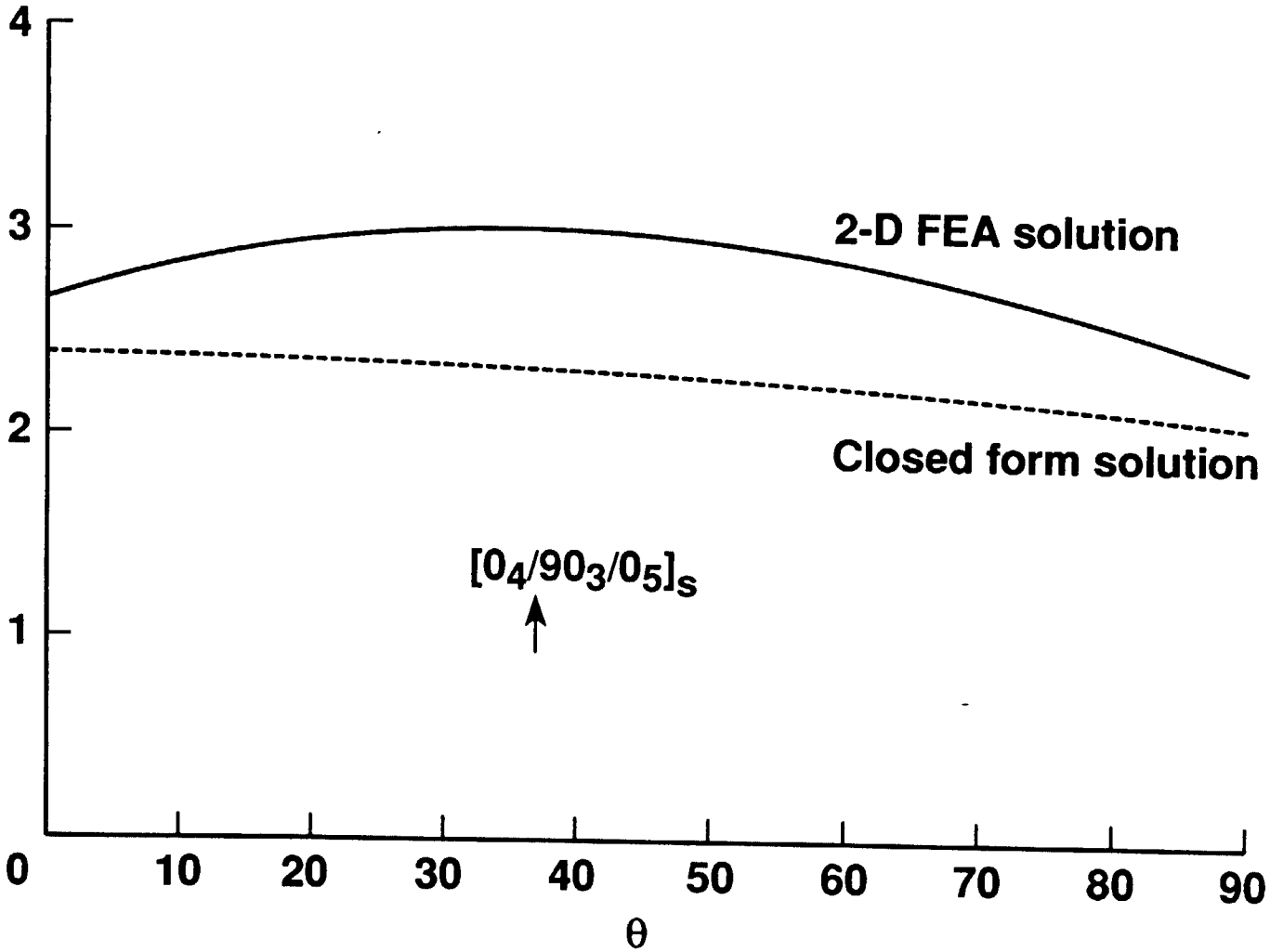


Fig. 14. - Tangential stress variation with theta.

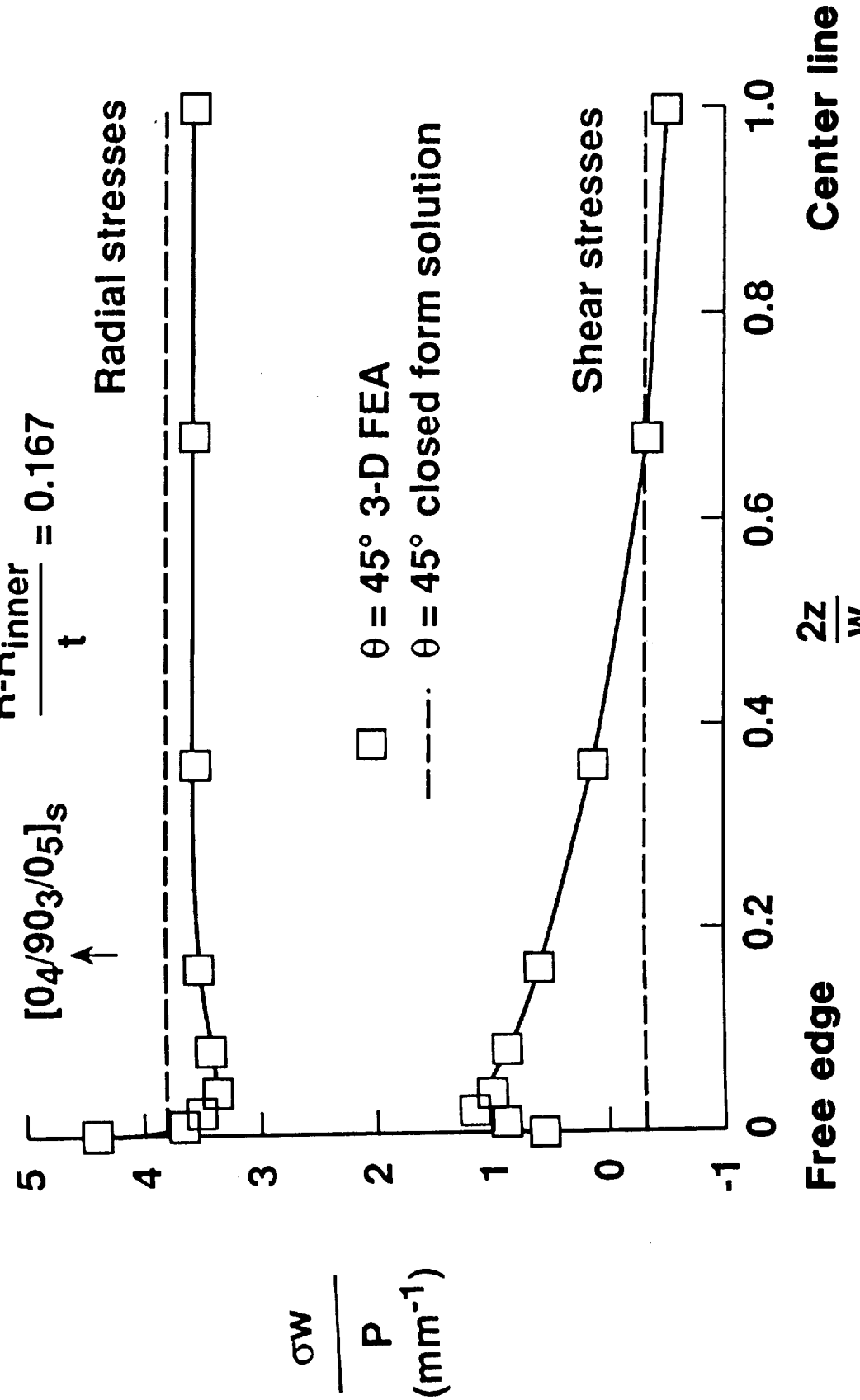


Fig. 15. - Radial and shear stress variation across width.

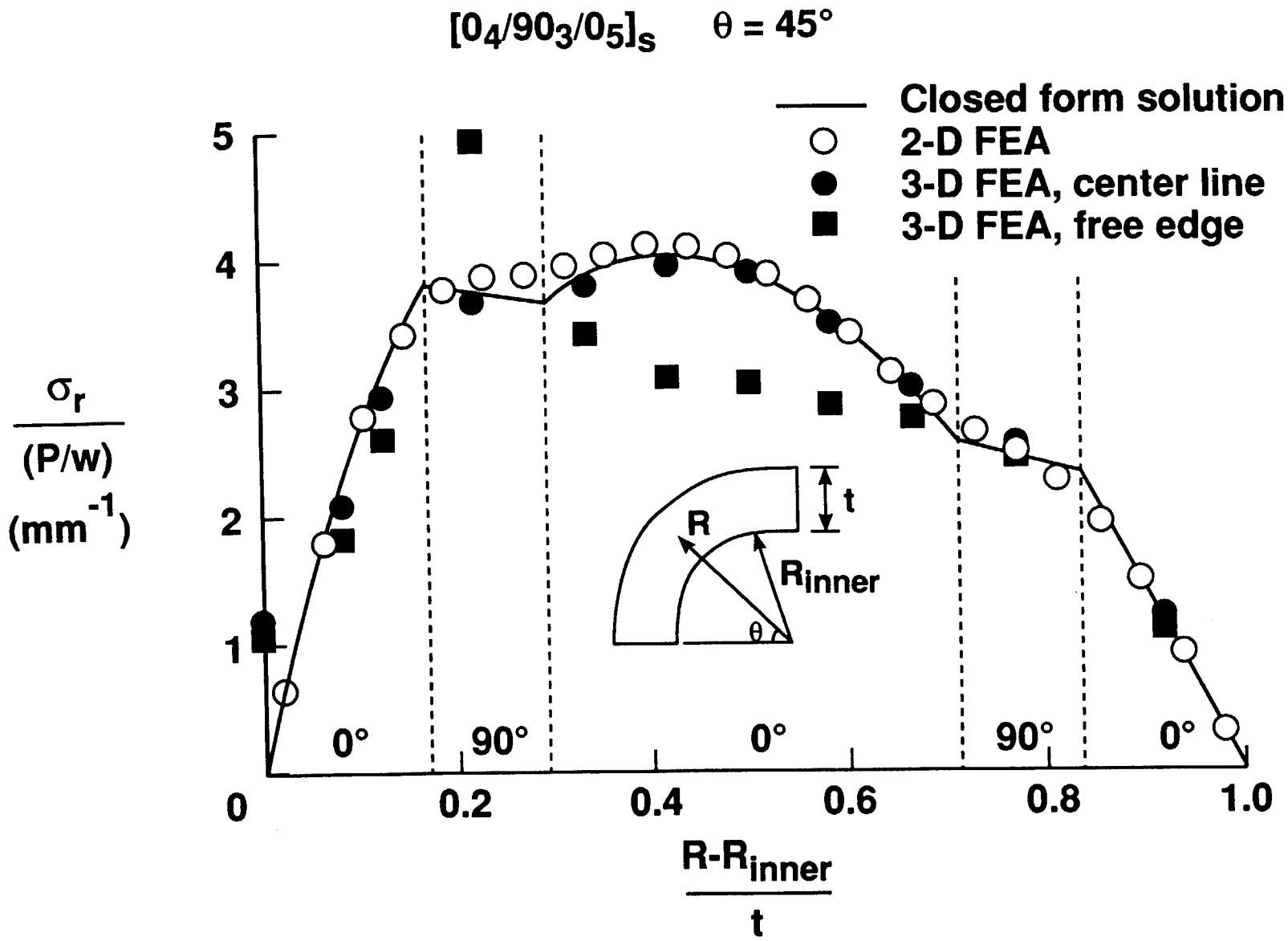


Fig. 16. - Radial stress through thickness.

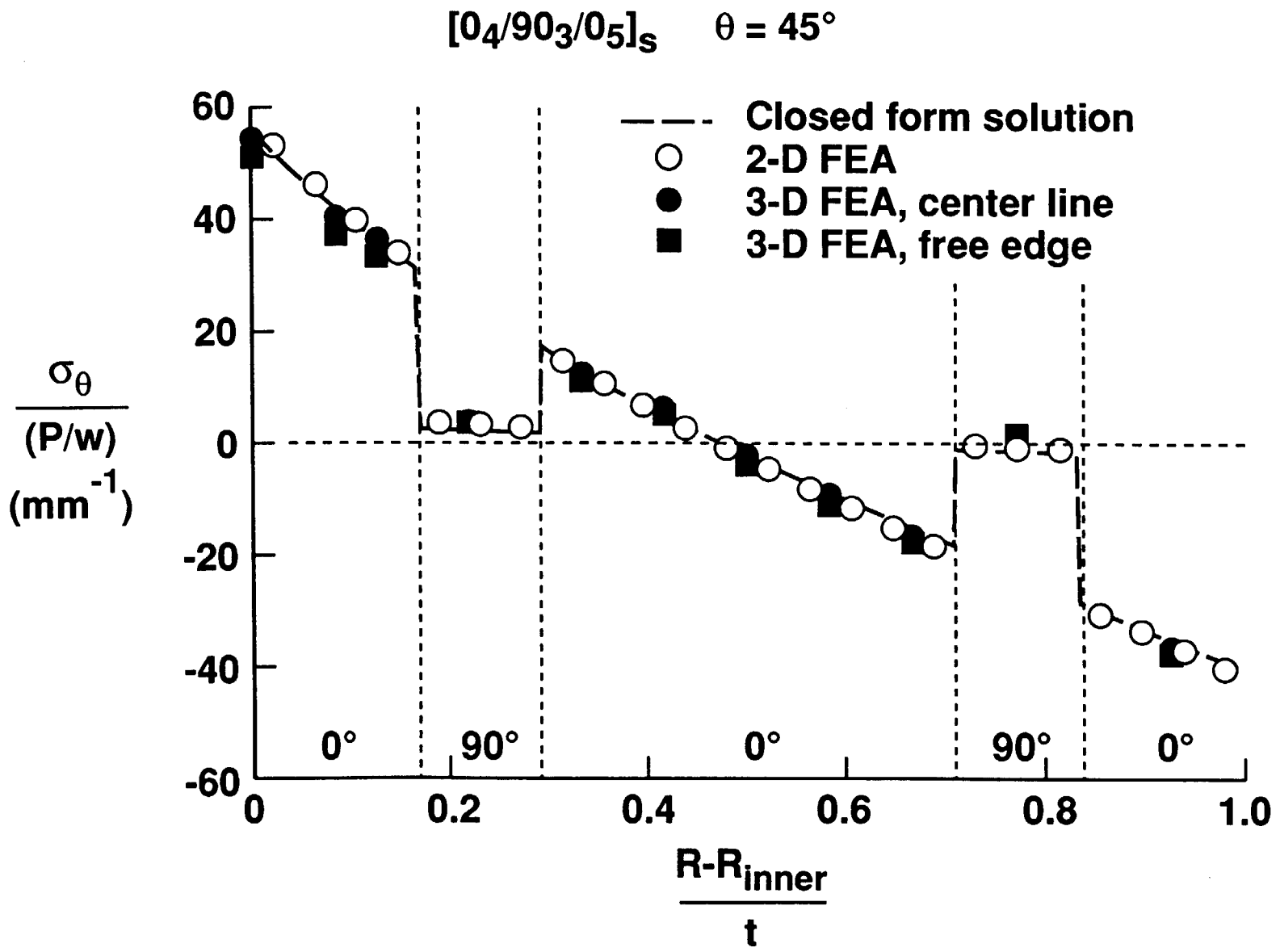


Fig. 17. - Tangential stress through thickness.

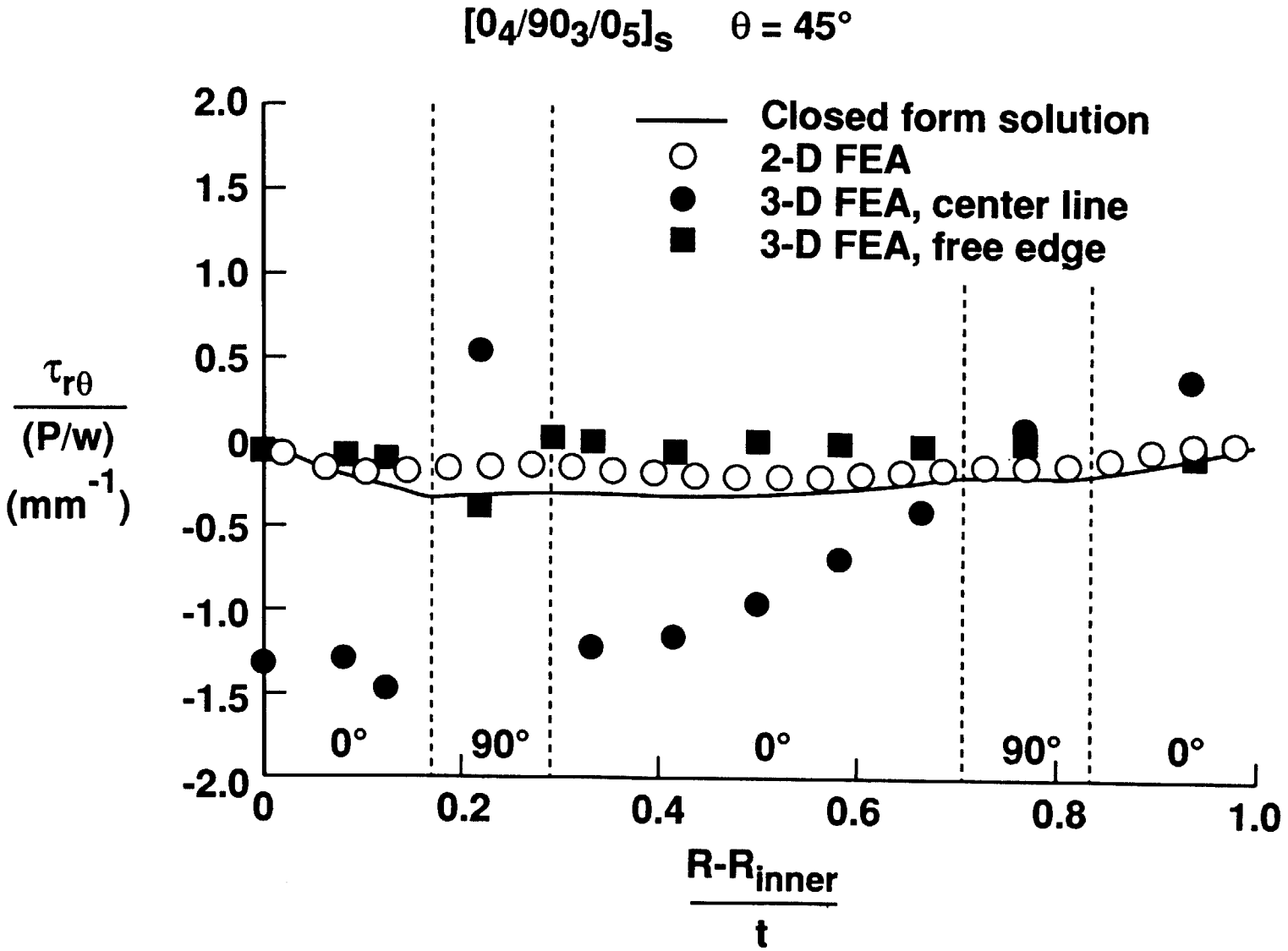


Fig. 18. - Shear stress through thickness.

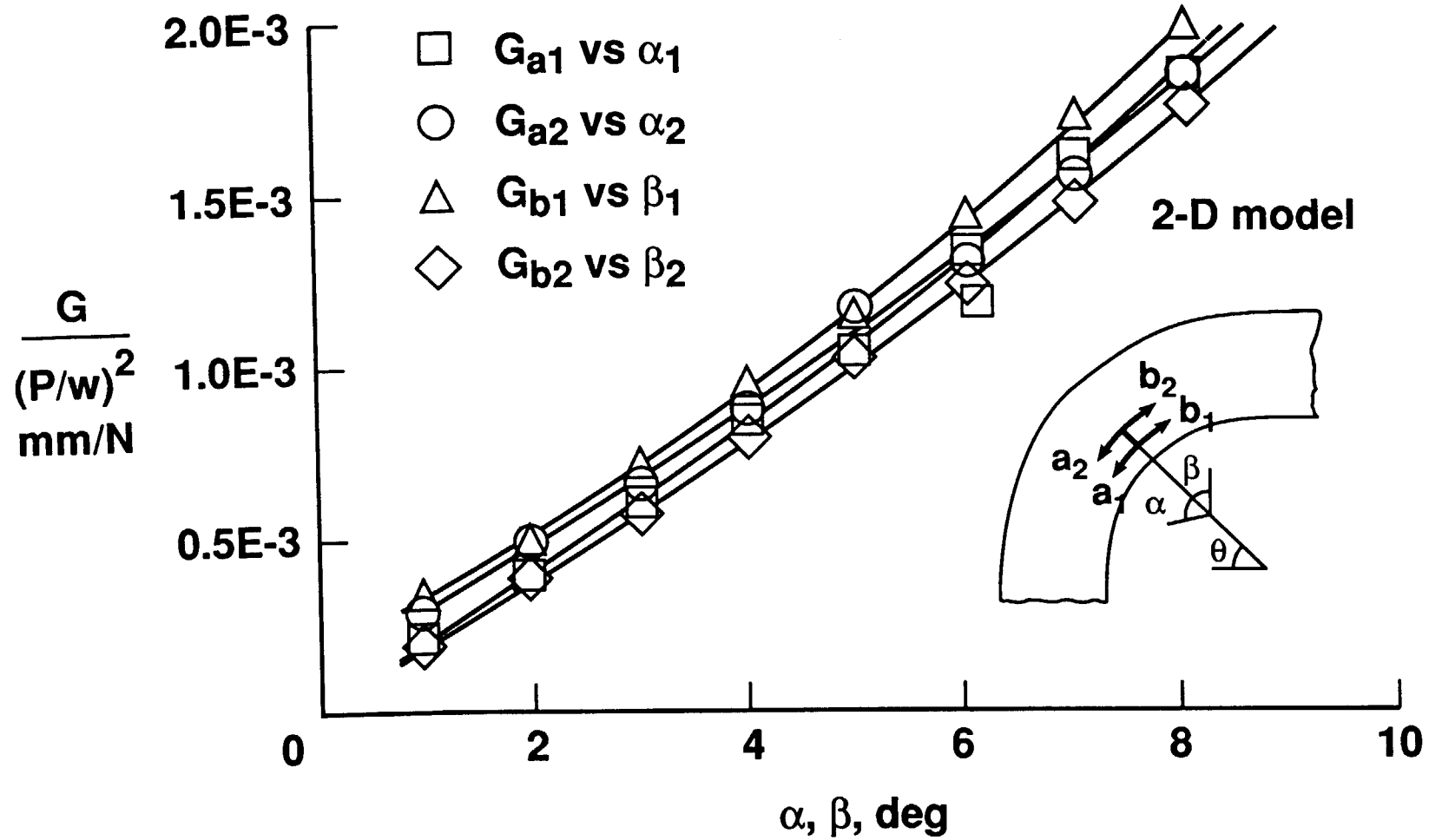


Fig. 19. - G variation with delamination growth along four paths for lay-up B.

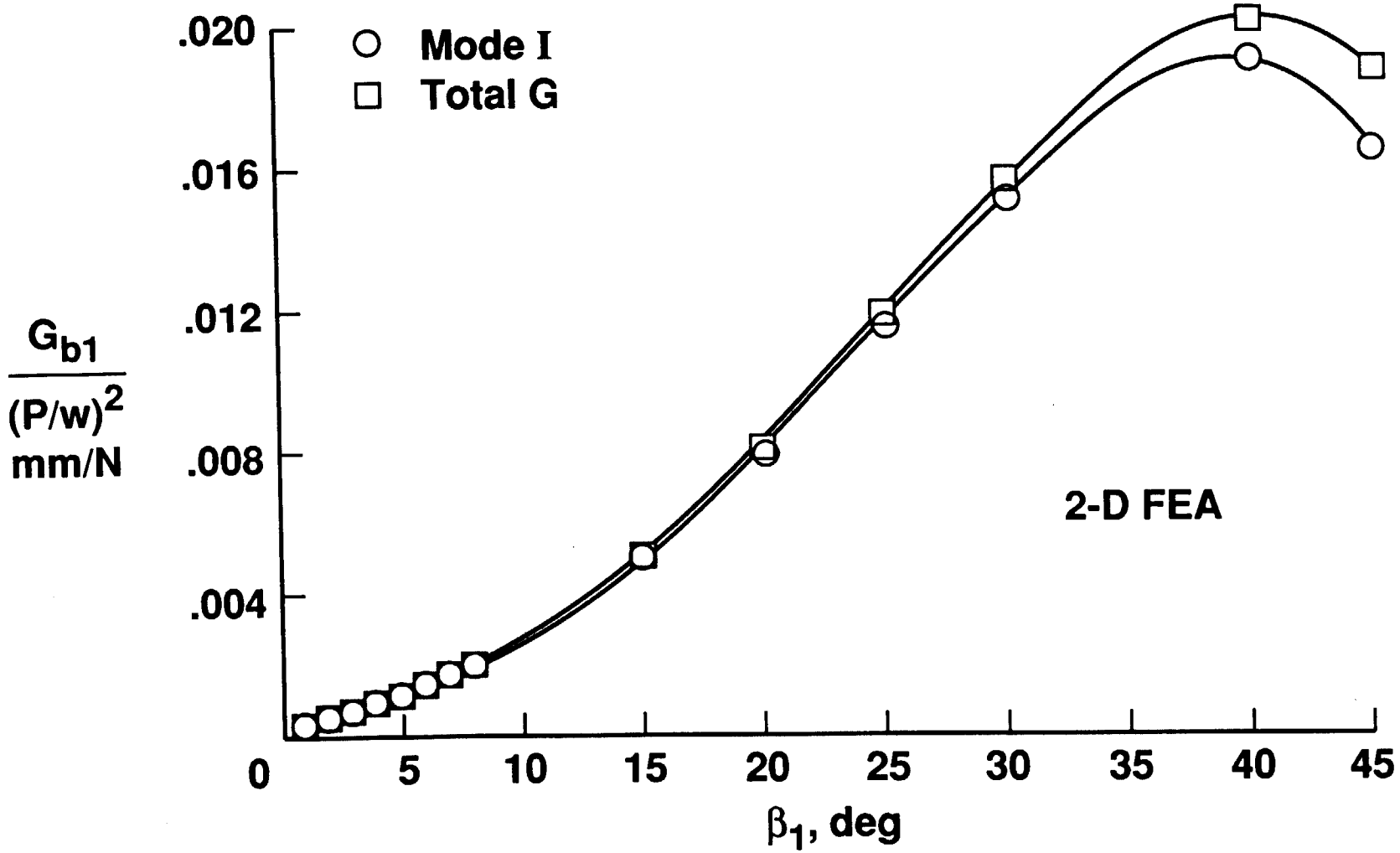


Fig. 20. - G variation along path $b_1$ for lay-up B.

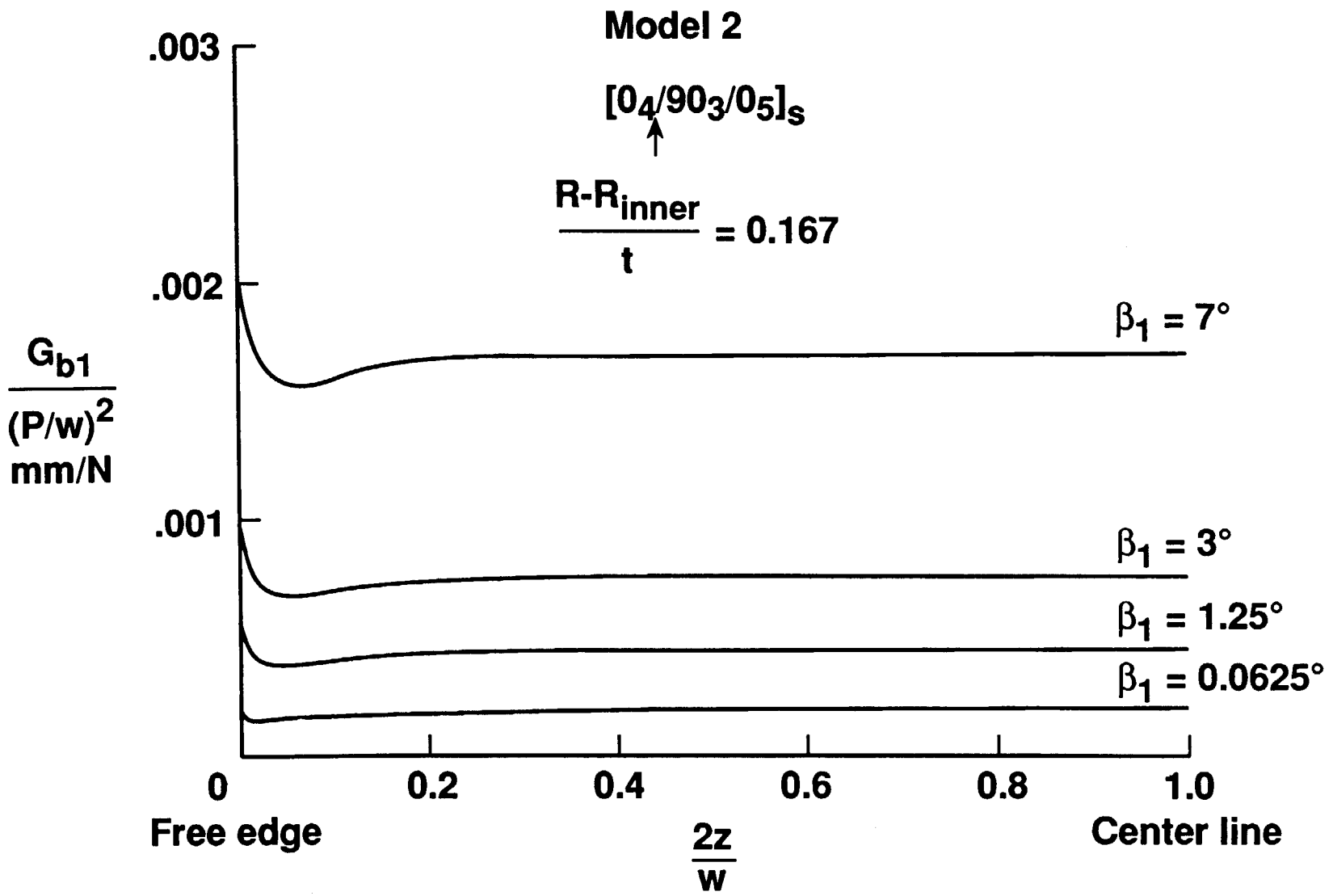


Fig. 21. - G variation across width at various delamination lengths.

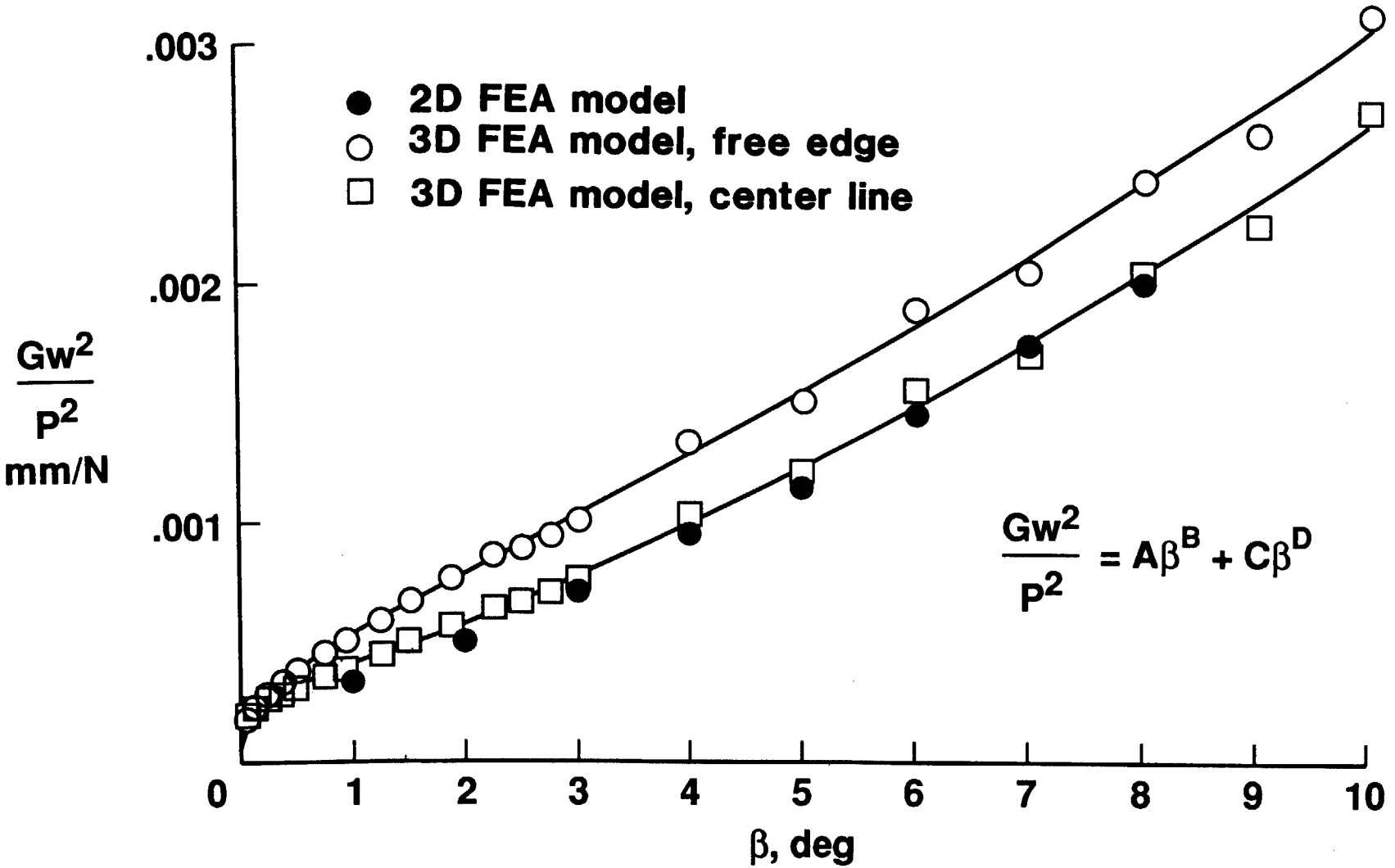


Fig. 22. - G variation with delamination growth close to matrix crack.

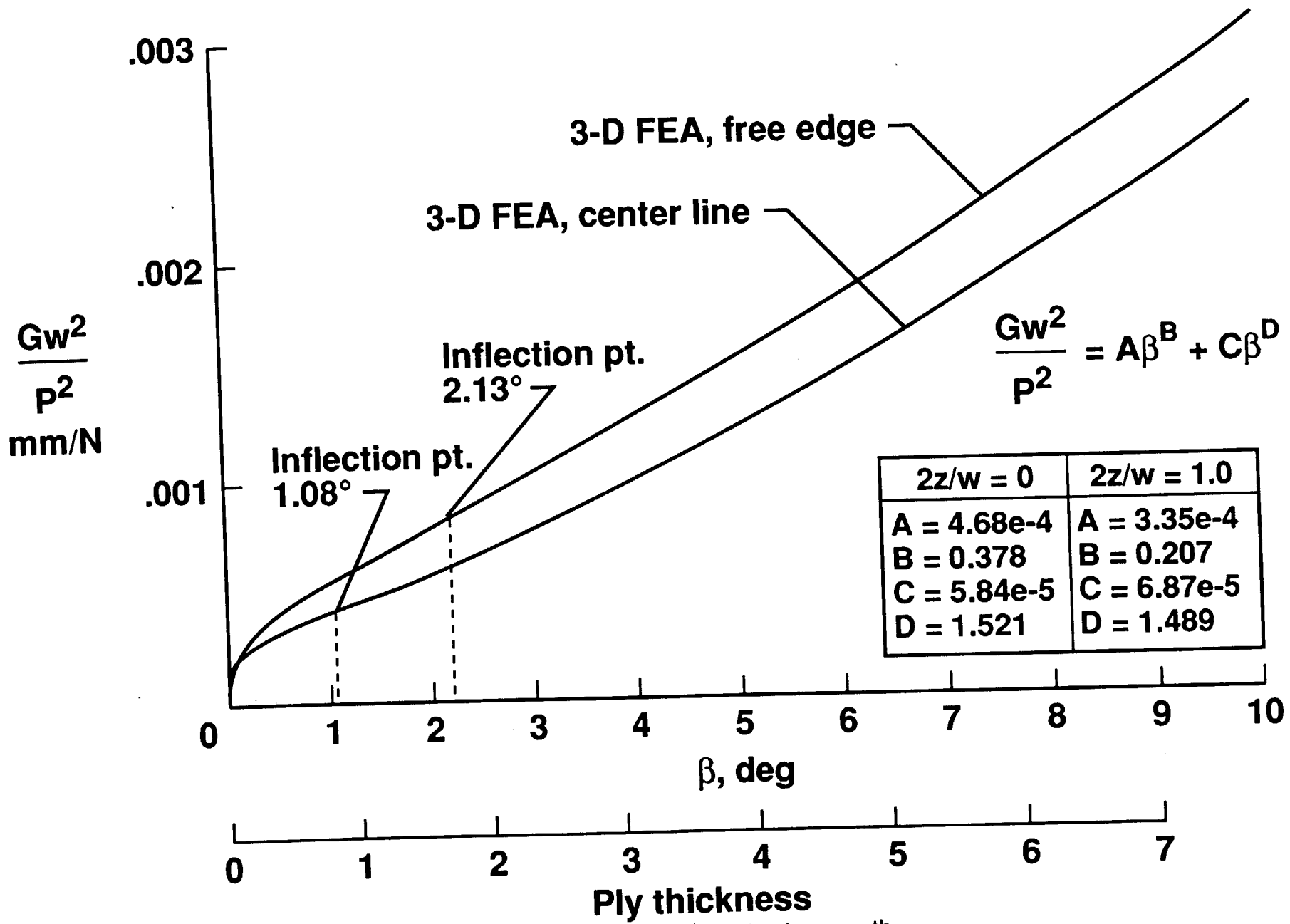


Fig. 23. - Curve fit of G variation with delamination growth.

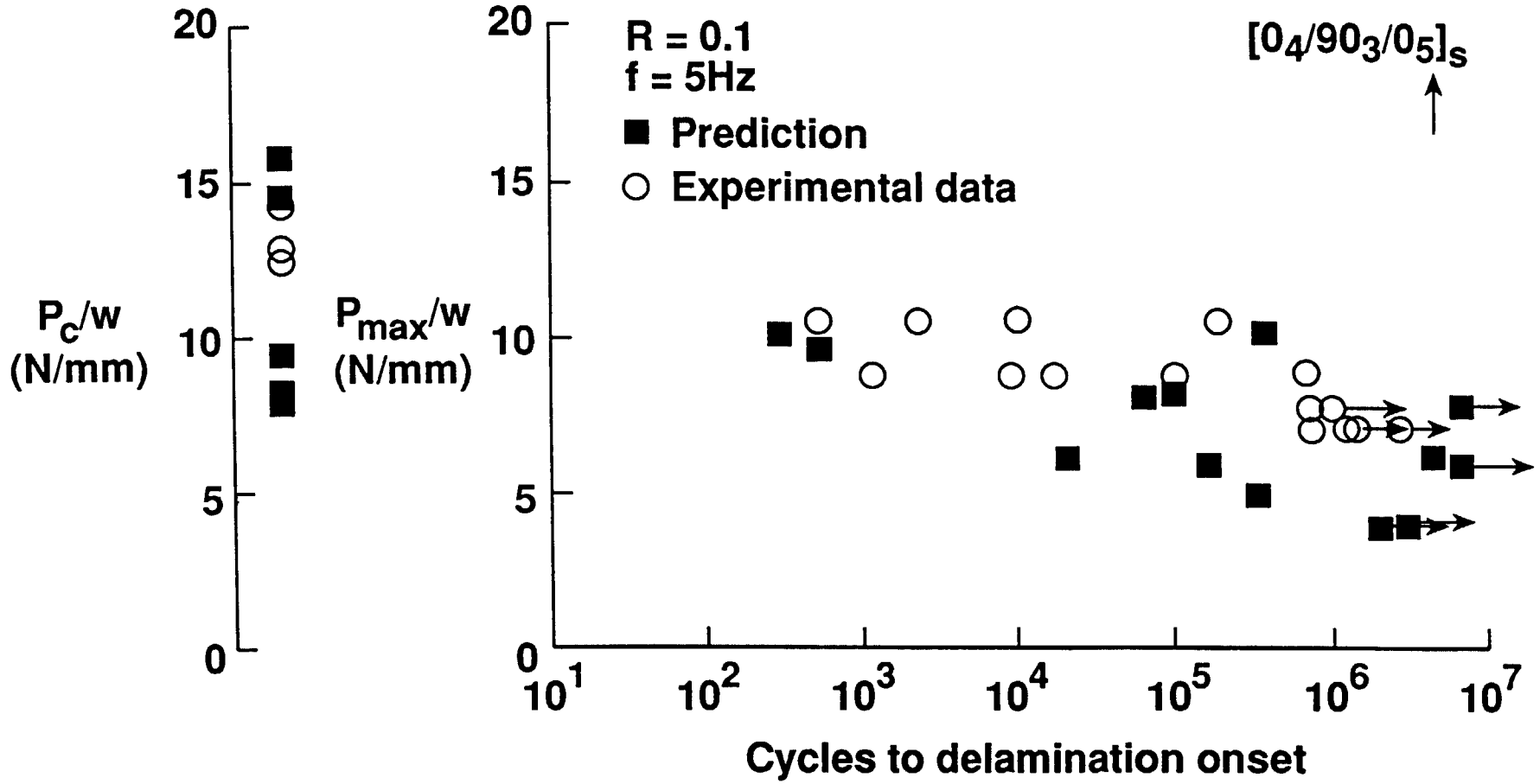


Fig. 24. - Prediction of interlaminar tension failure between 0° plies.

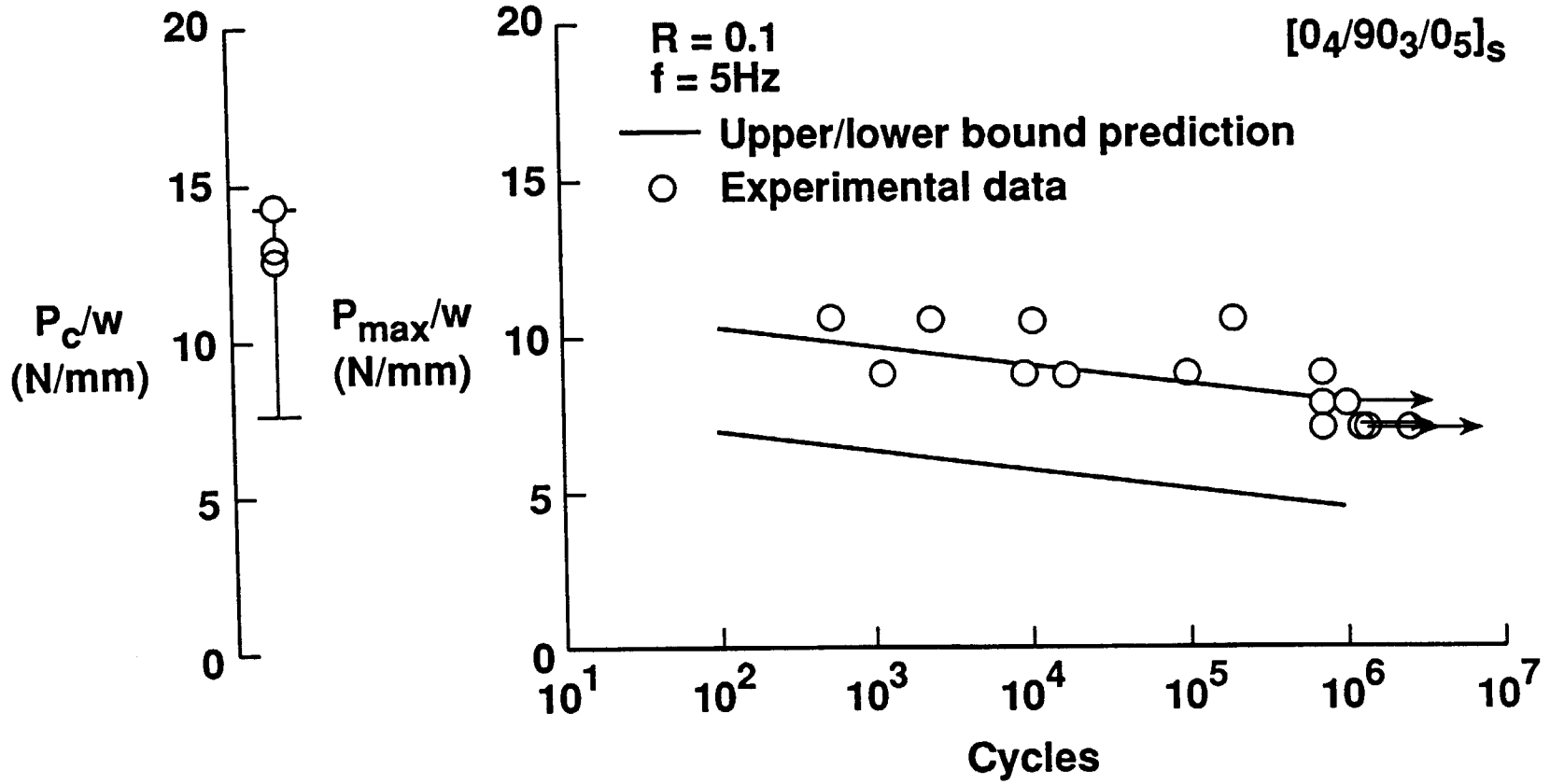


Fig. 25. - Prediction of transverse matrix cracking using the Tsai-Hill criterion.

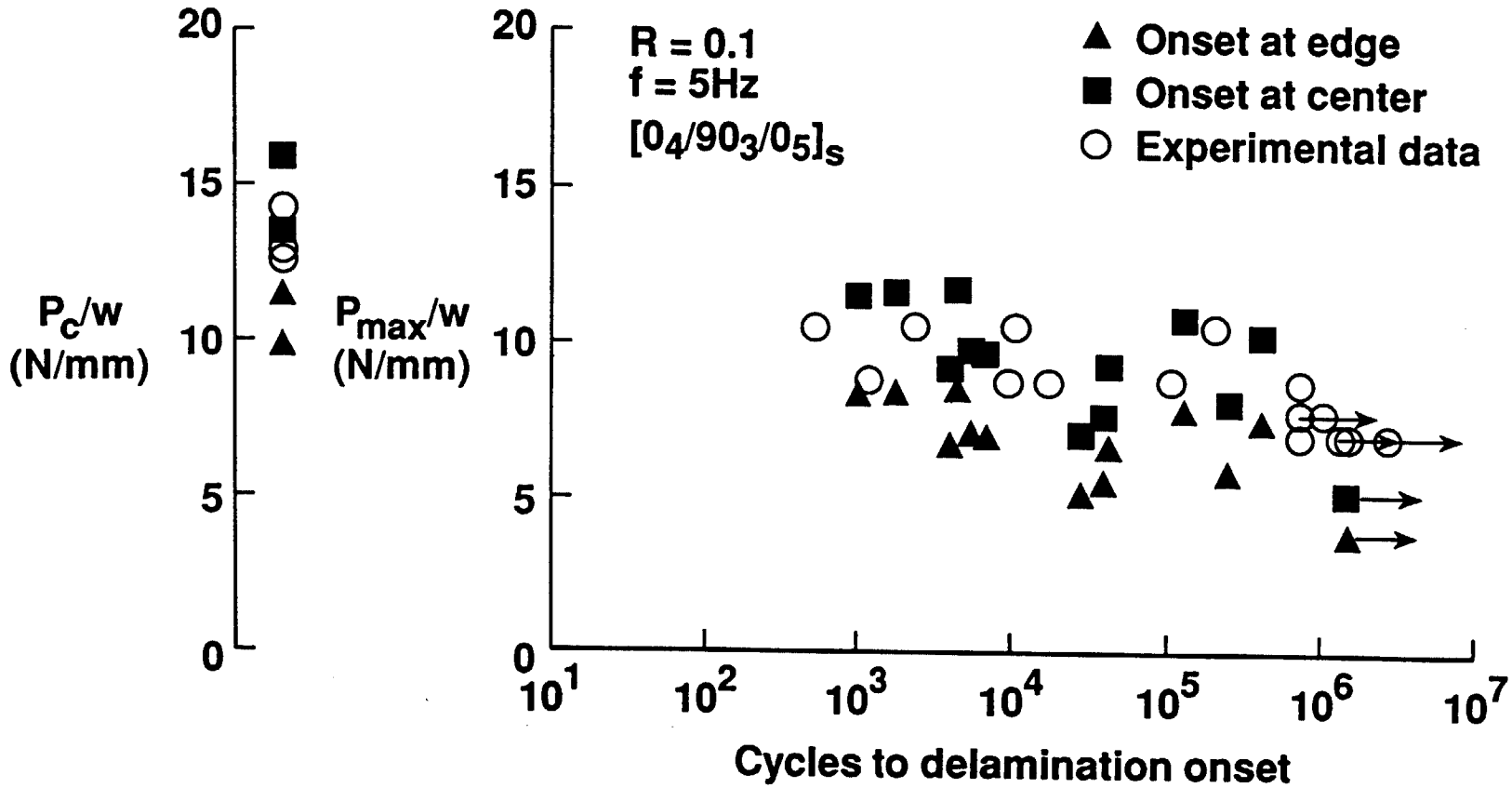


Fig. 26. - Prediction of delamination onset using fracture mechanics criterion.

NASA
National Aeronautics and Space Administration

# Report Documentation Page

| 1. Report No. | 2. Government Accession No. | 3. Recipient's Catalog No. |
|---|---|---|
| NASA TM-104089<br>AVSCOM TR-91-B-009 | | |

**4. Title and Subtitle**

Damage Prediction in Cross-Plied Curved Composite Laminate

**5. Report Date**

July 1991

**6. Performing Organization Code**

**7. Author(s)**

Roderick H. Martin* and Wade C. Jackson

**8. Performing Organization Report No.**

**10. Work Unit No.**

505-63-50-04

**9. Performing Organization Name and Address**

NASA Langley Research Center, Hampton, VA 23665-5225
U.S. Army Aviation Research and Technology Activity (AVSCOM)
Aerostructures Directorate
Hampton, VA 23665-5225

**11. Contract or Grant No.**

**13. Type of Report and Period Covered**

Technical Memorandum

**12. Sponsoring Agency Name and Address**

National Aeronautics and Space Administration
Washington, DC 20546
U.S. Army Aviation Systems Command
St. Louis, MO 63166

**14. Sponsoring Agency Code**

**15. Supplementary Notes**

*Analytical Services and Materials, Inc., Hampton, VA

**16. Abstract**

This paper details the analytical and experimental work required to predict delamination onset and growth in a curved cross-plied composite laminate subjected to static and fatigue loads. The composite used was AS4/3501-6, graphite/epoxy. Analytically, a closed form stress analysis and 2-D and 3-D finite element analyses were conducted to determine the stress distribution in an undamaged curved laminate. The finite element analysis was also used to determine values of strain energy release rate at a delamination emanating from a matrix crack in a 90° ply. Experimentally, transverse tensile strength and fatigue life were determined from flat 90° coupons. The interlaminar tensile strength and fatigue life were determined from unidirectional curved laminates. Also, mode I fatigue and fracture toughness data were determined from double cantilever beam specimens. Cross-plied curved laminates were tested statically and in fatigue to give a comparison to the analytical predictions. A comparison of the fracture mechanics life prediction technique and the strength based prediction technique is given.

| 17. Key Words (Suggested by Author(s)) | 18. Distribution Statement |
|---|---|
| Composite materials<br>Curved laminate<br>Delamination<br>Strain energy release rate | Unclassified - Unlimited<br>Subject Category - 39 |

| 19. Security Classif. (of this report) | 20. Security Classif. (of this page) | 21. No. of pages | 22. Price |
|---|---|---|---|
| Unclassified | Unclassified | 53 | A04 |